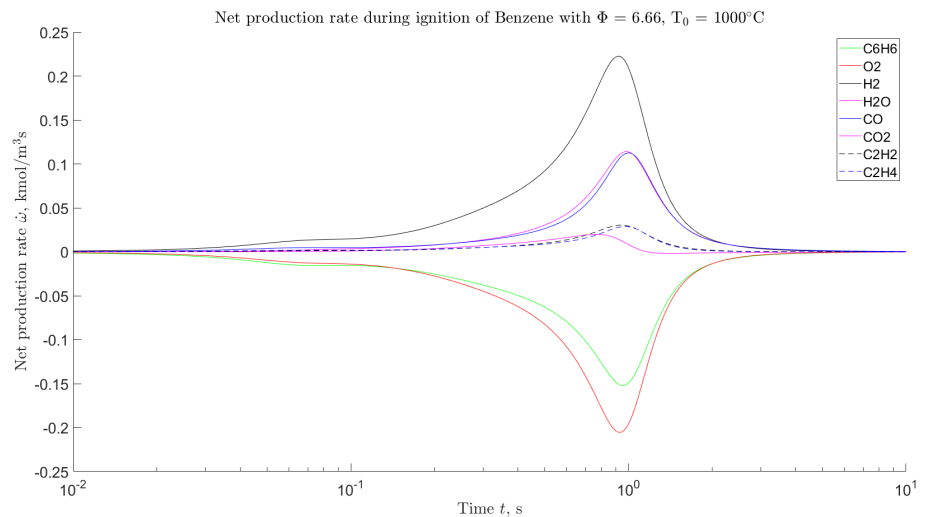Håkon Dalbakken

Safety Aspects of Organic Rankine Cycles (ORC) with Combustible Working Fluids

Master's thesis in Mechanical Engineering
Supervisor: Ivar S. Ertesvåg
Co-supervisor: Lars O. Nord

June 2021

Master's thesis

NTNU
Norwegian University of Science and Technology

Håkon Dalbakken

Safety Aspects of Organic Rankine Cycles (ORC) with Combustible Working Fluids

Master's thesis in Mechanical Engineering
Supervisor: Ivar S. Ertesvåg
Co-supervisor: Lars O. Nord
June 2021

Norwegian University of Science and Technology
Faculty of Engineering
Department of Energy and Process Engineering

NTNU
Norwegian University of
Science and Technology

Abstract

Despite the long history of organic Rankine cycles (ORC), there is limited research on these cycles operating with subatmospheric pressure. Subatmospheric pressures enables higher pressure ratios and consequently higher cycle efficiency, but is avoided mainly due to the combustion risk if ambient air was to breach into the system. This thesis aims to perform a theoretical investigation of the consequences of allowing air into an organic Rankine cycle operating with subatmospheric pressure on the low-pressure side. The cycle was designed to use n-pentane or benzene as working fluid, with condenser outlet temperature set to 30°C and evaporator outlet temperature set to 150°C.

The methodology used to investigate this matter was divided into two categories; non-reacting and reacting flow. Methodology for non-reacting flow was developed in this thesis. Mainly from three doctoral theses, and supplied by original analysis. An inleak model was formulated, with the main variable being the pressure of the gas phase on the low-pressure side. The main outputs were relations for the molar fraction of air on both pressure sides. When investigating two-phase flow in the pump it was found that phase separation can occur, and gas can accumulate at the pump inlet, effectively blocking it.

Methodology for reacting flow was taken from a textbook on combustion, this thesis did not contribute to any combustion theory. The equivalence ratio Φ was formulated as a function of gas phase pressure. The computational toolbox Cantera was used with Matlab and Python to simulate ignition and flame structures. A detailed kinetic mechanism from the research group CRECK was used in these simulations. It was found that an organic Rankine cycle with benzene used as working fluid is exposed to combustion on the low-pressure side at given temperatures. The cycle using n-pentane as working fluid is not exposed to combustion. The two working fluids had different results due to their respective saturation pressures being significantly different.

A procedure to determine if a working fluid is safe or unsafe regarding combustion was developed. This procedure calculates the equivalence ratio for a wide range of conditions, uses the condition with the value of Φ closest to unity, and simulates combustion processes at that condition. Post-processing of simulation data is required to determine whether combustion occurs or not, under those conditions. It was concluded that more research is needed, both in terms of validating developed models, but also on feasibility of subatmospheric organic Rankine cycles.

Samandrag

Trass i at organiske Rankine-syklusar (ORC) har eksistert ei stund, er det lite forsking på slike syklusar der subatmosfærisk trykk blir brukt. Subatmosfærisk trykk opnar for høgare trykkforhold som igjen gjev høgare verknadsgrad. Slike trykk er unngått då det er risiko for forbrenning dersom det trengjer luft frå omgjevnadane inn i systemet. Denne avhandlinga har som mål å gjere ei teoretisk undersøking av konsekvensane ved å ha luftstrøyming inn i ein organisk Rankine-syklus med subatmosfærisk trykk på lågtrykk-sida. Syklusen var sett til å bruke n-pentan eller benzen som arbeidsmedium. Utløpstemperatur til kondensator er sett til 30°C, utløpstemperatur til dampkjelen er sett til 150°C.

Metoden som vart brukt for å undersøkje problemstillinga vart delt inn i to kategoriar, ikkje-reaktiv og reaktiv strøyming. Metode for ikkje-reaktiv strøyming vart etablert i denne avhandlinga. Mykje av teorien er henta frå tre doktoravhandlingar, anna teori er funne ut av undervegs. Ein modell der luft kan trengje inn i syklusen, med trykket til gassfasen på lågtrykk-sida som fri variabel, vart etablert. Hovudresultata frå denne modellen var relasjonar for molfraksjonen av luft på begge trykksidene av syklusen. Undersøking av tofase-strøyming i pumpa viste at fase-separering kan skje, og at gassfasen kan samle seg ved inntaket til pumpa, som til slutt blokkerer den.

Metode for reaktiv strøyming er henta frå ei lærebok om forbrenning, her er det ingen bidrag til forbrenningsteori. Eit uttrykk for Φ vart formulert som funksjon av trykket til gassfasen på lågtrykk-sida. Berekningsverktøyet Cantera var tatt i bruk med Matlab og Python for å simulere tenning og flammestrukturar. Ein detaljert kinematisk mekanisme frå forskningsgruppa CRECK var tatt i bruk i desse simuleringane. Eit viktig funn var at ein organisk Rankine-syklus som har benzen som arbeidsmedium er utsett for forbrenning på lågtrykk-sida ved den gitte tilstanden. Syklusen som brukte n-pentan som arbeidsmedium er ikkje utsett for forbrenning. Dei to arbeidsmedia hadde ulike resultat grunna svært ulike mettingstrykk.

Det vart etablert ein metode for å avgjere om eit arbeidsmedium er trygt å bruke eller ikkje, med tanke på forbrenning. Denne metoden reknar Φ for ei rekke tilstandar, tilstanden som gir Φ nærast 1 vert brukt i forbrenningssimulering. Analyse av data frå simulering er eit krav for å avgjere om forbrenning skjer eller ikkje, i den tilstanden. Konklusjonen var at det er behov for meir forsking, blant anna på validering av nye metodar, men også på gevinstane av å ha subatmosfærisk trykk i organiske Rankine-syklusar.

Contents

INTRODUCTION

The ever-increasing demand of electrical energy brings numerous challenges, increasing efficiency of thermal power plants is one of them. A great source of potential is the thermal energy found in exhaust gases as this is often ejected to the atmosphere, as investigated by Papaetrou *et al.* [1]. Gas ejected at low temperatures (100°C - 200°C) is hard to utilize with traditional steam vapor power cycles such as the Rankine cycles. Organic Rankine cycle (ORC) are more appropriate here.

Although organic Rankine cycles have been around for a while, they are often designed with a lower pressure constraint. The pressure must be a bit above atmospheric pressure to avoid ambient air leaking into the cycle. The reason for this is that having air leak into a cycle where organic fluids are present may produce mixtures that are easily flammable, and combustion processes may be trapped inside the pipes. Traditional Rankine cycles using water do not have this problem, and are constrained by material properties rather than risk of air inleak. Having such a strict condition on the organic Rankine cycles limits the operating range and cycle efficiency. One may obtain higher efficiencies if the low-pressure side was not constrained, but is that safe?

1.1 Scope of work

The scope of this thesis is set by the given task description, found in the Appendix (Norwegian only). This thesis is a scientific report on the work conducted by the author on subatmospheric organic Rankine cycles, regarding air inleak and combustion properties. The scope of work includes:

- Performing a literature review on subatmospheric organic Rankine cycles, or related subjects. Performing literature reviews on relevant fields of study.

- Developing a simple theoretical organic Rankine cycle with appropriate working fluids.

- Investigating how a simple, theoretical organic Rankine cycle and its components are affected when air is allowed to enter the cycle at specified locations.

- Using process simulators to simulate a thermodynamic model of the cycle when air is present.

- Performing simulations on combustion processes using appropriate software and a detailed kinetic mechanism.

- Draw conclusions on the safety aspects of organic Rankine cycles with combustible working fluids.

The following tasks are excluded from, or beyond the scope due to lack of time, funds, laboratories, or it simply not being relevant:

- Performing organic Rankine cycle design with respect to efficiency or thermoeconomics.

- Investigating the advantages of using subatmospheric pressures in cycles. No computations are performed with the intention to state that reducing pressures below atmospheric will increase efficiency.

- Investigating safety aspects not related to combustion such as poisoning, pollution, or environmental impact.

- Performing experiments on physical components in a laboratory

1.2 Main objective

"What are the consequences of allowing air into an organic Rankine cycles operating with a subatmospheric pressure?"

The question above attempts to summarize the main objective of this thesis in one sentence. The main goal is to explore safety aspects of organic Rankine cycles where the low-pressure side is subatmospheric and air leaks in. Risk and consequences of combustion inside the cycle are central parts of these safety aspects. The rather broad question posed initially, is decomposed into specific questions and objectives, which allows for a better overview of which tasks to complete. The reader will also benefit from this as it is easier to keep track of what is going on in each section. Another measure taken to aid the reader is keeping a red thread throughout the thesis and indicate how the current section contributes to the bigger picture.

1.2.1 Non-reacting flow

The first part of the thesis will present a basic organic Rankine cycle and investigate how air mixed into the working fluid affects the properties of the cycle. A mixture where no combustion is occurring is still of interest as there may be phase changes before any heat is added, for instance. The following questions are to be investigated:

- How will mixing with air change the thermodynamic properties of the working fluid and the cycle?

- Is there a limit to how much air the pump can handle before the cycle stops?

A huge challenge to come when evaluating this non-reacting mixture is that there may be two-phase flow through the various equipment in the cycle. Liquid-gas flow is subject to modern research, and is especially in turbomachinery a challenge in the oil and gas industry.

1.2.2 Reacting flow

The second part of the thesis deals with reacting mixtures. Complete analysis of combustion is to be performed with detailed mechanisms of how the molecules change as the combustion occurs. This will enable analysis of a possible scenario where sparks from a turbine ignites air-hydrocarbon mixtures and a flame develops. The following questions are to be investigated:

- Can the mixture of air and working fluid ignite at specific locations in the cycle?

- Can ignition of this mixture create a self-sustaining flame?

- What are the consequences of reacting mixtures in the cycle?

A detailed kinetic mechanism enables analysis of ignition and flame structures at various values of the air/fuel ratio. With the equivalence ratio Φ, the properties of combustion can be linked to the amount of air leaking into the cycle. If there is a limit to how much air the pump can handle before it is unable to drive a flow, this limit can be imposed on the combustion analysis, indicating a minimum value for Φ. To avoid expensive numerical simulations all computations related to combustion are performed in one dimension only, this dimension is either time or pipe directional axis.

1.2.3 Discussion and conclusion

Finally, the results from the individual investigations will be evaluated in relation to each other and in relation to the main objective. This discussion seeks to bring a conclusion regarding the risk and consequences of operating an organic Rankine cycle at a subatmospheric pressure. An evaluation of the quality of the assumptions and developed models is to be performed to point out weak parts of the methods used that may not hold in a real world case. Finally, some points regarding the future outlook of the main objective is made. This thesis is in no way more than a first step towards exploring subatmospheric organic Rankine cycles with combustion aspects.

1.3 Relevant studies and literature

Organic Rankine cycles and combustion are both well-established fields of study where major amounts of papers are published in journals every year. Studies evaluating subatmospheric organic Rankine cycles are less common, however. The main objective is evaluating safety aspects related to subatmospheric organic Rankine cycles, an extensive search in available literature reveals that few major publications on this topic are easily available. The publications that do exist, are either of restricted access or does not contain the correct keywords. Due to the lack of literature this thesis will make use of available literature on the specific parts mentioned when decomposing the main objective. Relevant literature may be textbooks, doctoral theses, and published articles:

Organic Rankine cycles: *Organic Rankine Cycle Power Systems: Technologies and Applications* 1st Ed. 2017, by Macchi & Alstofi [2], describes organic Rankine cycles in detail and how they are implemented in various scales. The textbook contains references to many case studies, doctoral theses, and other papers. Chapter 18 provides an overview of research done on systems of smaller case.

Thermodynamics of mixtures: *Principles of Engineering Thermodynamics* 8th Ed. 2015, by Moran *et al.* [3], is an introduction to thermodynamics for undergraduate students. Chapters 11, 12 and 14 covers thermodynamics of mixtures, equations of state, and phase equilibrium. Peng & Robinson (1976) [4] provides information regarding an equation of state for mixtures. Much process simulation is done in the process simulator *Aspen Hysys* and its theory guide [5] covers how the simulator performs various operations.

Pumping: The doctoral theses of Aoun (2008) [6] and Clemente (2013) [7] discuss, among other things, how different types of pumps perform in organic Rankine cycles of different scales. The doctoral thesis of Serena (2016) [8] includes experiments on multiphase pumps where air is mixed into the liquid stream and pumped. Information gathered from these may help determine how the pumping work changes as more air is introduced.

Combustion: *An Introduction to Combustion: Concepts and Applications* 4th Ed. 2020, by Turns [9], is an introduction to basic modeling of ignition and flame structures. Chapters 4 and 5 introduces kinetic mechanisms and chapter 8 presents laminar premixed flames. Numerical solution of the equations presented is performed in the mathematical programming software *Matlab* [10] by using the open-source toolbox *Cantera* [11].

Kinetic mechanisms: Combustion research conducted by scientists at the *CRECK* modeling group at *Politecnico di Milano* [12]. Various models are available depending on which substances are of interest and temperature range. Papers written by the scientists will assist in the choice of kinetic model.

1.4 How to read the thesis

The thesis is divided into sections. Methodology covers two very different subjects and is therefore split into two sections, these sections are further split into topics. As mentioned, it is desirable to have a step-wise procedure when developing the methodology. The results are grouped by non-reacting and reacting mixture. Some results from non-reacting mixture analysis may be repeated a few times due to their importance. The table of contents lists the various sections and topics, the two following sections contains core methodology and results, followed by a discussion and finally a conclusion.

1.5 Acknowledgements

The author wishes to acknowledge the supervisor of this thesis, professor Ivar S. Ertesvåg, for his specialization course on combustion, recommendations on kinetic mechanisms, and general advice on writing a thesis. Professors Lars O. Nord and Lars E. Bakken are also thanked for recommendations on relevant literature.

CYCLE MODELING

Air leaking into the cycle brings two challenges. The first is that the working fluid is now multi-component and two-phase at the pump inlet. This has influence on many properties of the cycle, such as pump work, evaporation pressure and efficiency. This section will present a model for the cycle and explore how these properties change depending on how much air is leaking in, with the pump model being a major point of discussion. Process simulation in Aspen Hysys is also to be presented.

2.1 Organic Rankine cycles

Understanding how a Rankine cycle works and how the organic working fluids is chosen is crucial to proceed in this chapter. It is expected that the reader is familiar with basic thermodynamics, i.e. the conservation laws and property relations.

The Rankine cycle is the cornerstone in power-generating systems based on phase-change (also called vapor power systems). A summarized description from [2] is given below:
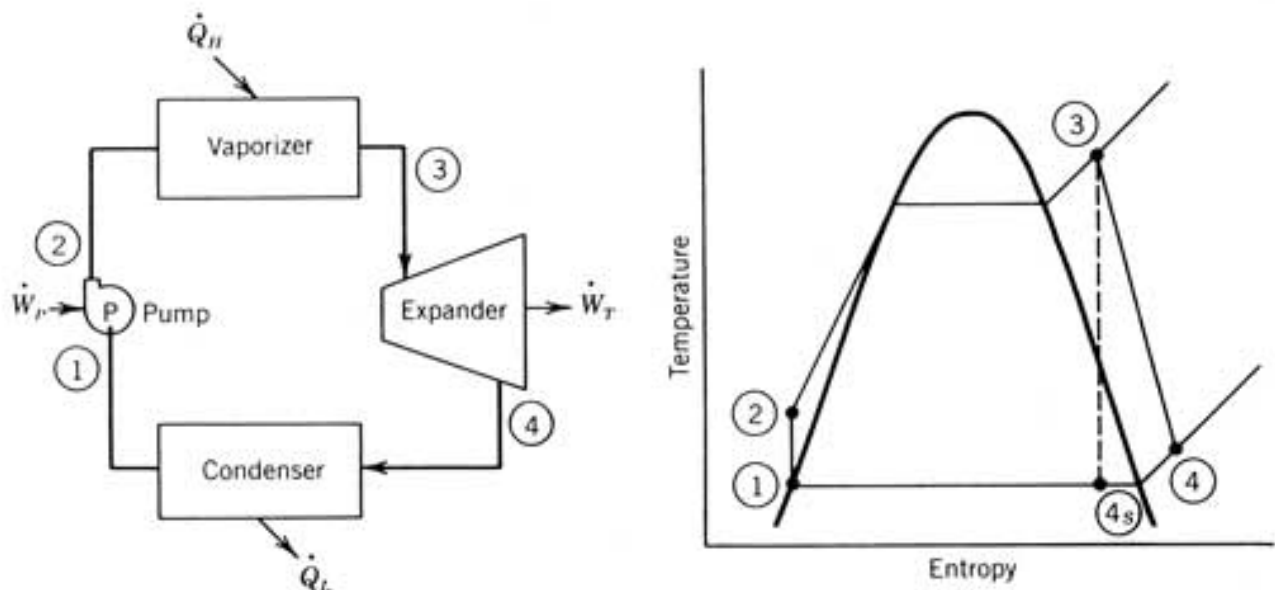

Figure 2.1: Schematic and temperature-entropy diagram of a basic Rankine cycle, figure from [13].

Rankine cycles exploit the fact that a change in pressure for a fluid in vapor phase requires more work than the same change in pressure for a fluid in liquid phase. By building up pressure in liquid phase and expanding in vapor phase, a net mechanical power can be extracted from the cycle. This requires a source and a sink for thermal energy, as the fluid must evaporate and condensate. All major components and their connections in the cycle can be seen the left part of Fig. 2.1. The right part of Fig. 2.1 illustrates how properties of the fluid changes throughout the cycle in a temperature-entropy diagram.

1. Saturated liquid, regarded as the reference point in the cycle.

2. Compressed/subcooled liquid, from State 1 in Fig. 2.1 the pressure of the liquid is raised in a pump. This pressure relates to evaporation temperature.

3. Superheated vapor, from State 2 the fluid is heated in two or three steps: From subcooled to saturated liquid, from saturated liquid to saturated vapor, and optionally from saturated vapor to superheated vapor.

4. Superheated vapor, from State 3 the vapor is expanded in a turbine. In many cases the properties of this state depends on cycle design. Superheating to a high temperature leads to State 4 being superheated vapor. Less superheating in State 3 can lead to State 4 being a mix of saturated liquid and vapor when using ideal models, see point 4s in Fig. 2.1.

Fig. 2.1 is the general scheme of the cycle to be investigated in this study. The pump component will be analysed later in this section.

2.2 Base model

One of the main objectives of this study is to investigate how introducing air into an organic Rankine cycle affects its properties. To perform calculations, a mathematical model of a physical pump is needed This model contains all equations used to calculate properties of all states in the cycle. For convenience, the following terms are defined for this thesis:

- Mathematical model: Equations describing conservation of properties like mass and energy and property relations for the organic Rankine cycle.

- Base model: The mathematical model (and its equations) when no air is present in the cycle.

- Inleak model: The mathematical model when air is present in the cycle. Does also contain specific models for pumping-operation and phase transition.

  - Phase transition model: The part of the inleak model that handles phase transition.
  - Pump model: The part of the inleak model that handles the pumping operation.

2.2.1 Base cycle

A cycle equal to that illustrated in Fig. 2.1 is used and will hereby be referred to as the cycle. The main equations of this cycle are mass and energy conservation for control volumes, derived from mass conservation and the first law of thermodynamics:

$$\frac{dm_{CV}}{dt} = \sum \dot{m}_{in} - \sum \dot{m}_{exit} \tag{2.1}$$

$$\frac{dE_{CV}}{dt} = \dot{Q}_{CV} - \dot{W}_{CV} + \sum \dot{m}_{in} \cdot h_{in} - \sum \dot{m}_{exit} \cdot h_{exit} \tag{2.2}$$

where in is streams entering the control volume and $exit$ is streams leaving the control volume. These make up the mathematical model when the following assumptions are applied:

- Steady state process, steady flow where $d/dt = 0$.

- The fluid is saturated liquid at State 1 in Fig. 2.1.

- Evaporation and condensation are isobaric.

- Compression and expansion are adiabatic.

- Change in liquid density over the pump is negligible.

- Temperatures at condenser outlet and evaporator outlet are 30°C and 150°C, respectively.

2.2.2   Roadmap

With the base model introduced, a roadmap is drawn to outline which methodology to develop. The purpose of this map is to keep track of which results to use where, and will be referenced in the results section. Fig. 2.2 shows how the recently defined base model is used to choose working fluids, develop various models, and finally compare two models to draw a conclusion regarding cycle performance.
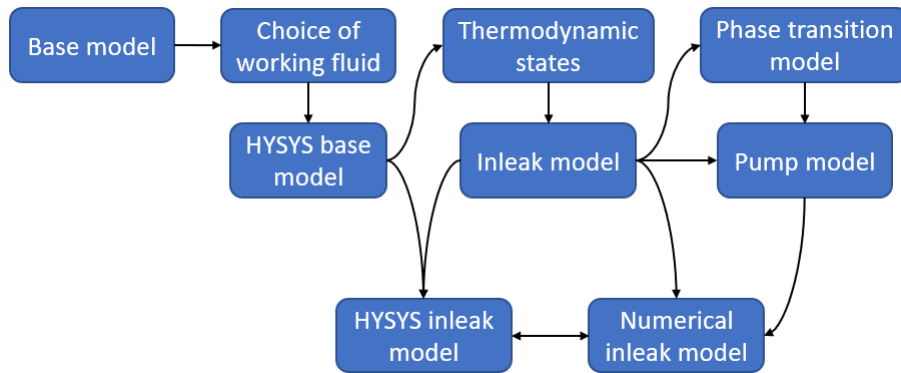
Figure 2.2: Roadmap of the methodology to be developed.

2.2.3   Choosing working fluid

Conventional Rankine cycles use water as working fluid. To operate and be efficient with low-temperature heat sources, another working fluid must be employed. Many organic substances have higher evaporation pressure for the same temperature, allowing for a higher pressure on the vapor side. Refs. [7] and [14] presents detailed procedures on the selection of working fluids for the interested reader. A few criteria relevant to this study[1] are used to select appropriate fluids:

---

[1]Cost of fluid, availability, and global warming potential are not considered here, although they are important parameters nonetheless.

Simple hydrocarbons: Analysis of chemical reactions in detail with limited time and computational resources calls for substances that have been researched thoroughly and are not too complex. This excludes fluorocarbons, hydrofluorocarbons, alcohols, cyclohexanes, etc. Only the simplest alkanes and benzene are considered.

Condensation temperature and pressure: The objective of this study is to investigate the scenario where air enters the cycle. The condensation pressure is the lowest pressure in the cycle, this must be subatmospheric for inleak to occur. The ambient temperature is assumed to below 30°C such that the working fluid is saturated liquid at 30°C at condenser outlet. Since the pressure is constant over the condenser, all working fluids must have $p_{sat} < p_{atm}$ at 30°C, light hydrocarbons like propane and butane are thus excluded.

Evaporation pressure: A low-temperature heat source is assumed to be above 150°C such that the working fluid is saturated vapor at 150°C at evaporator outlet. This sets the evaporation pressure, which cannot be extremely high, as various components in the cycle have a pressure rating. Evaporation pressure must still be above atmospheric to avoid air leaking in on both pressure sides. Evaporation pressure is assumed to be constant, meaning that all working fluids must have p_{sat} in the range 5-15 bar at 150°C.

2.2.4 Base model operation in Hysys

Aspen Hysys v10.0, hereafter referred to as just Hysys, is a commercially available software for process simulation. The simulator is widely used in fields such as the oil and gas industry. The cycle sketched in Fig. 2.1 is drawn in Hysys and simulated to find properties of interest, Fig. 2.3 is a screenshot of the cycle taken in Hysys. The simulation enables estimation of net power generation and overall efficiency.
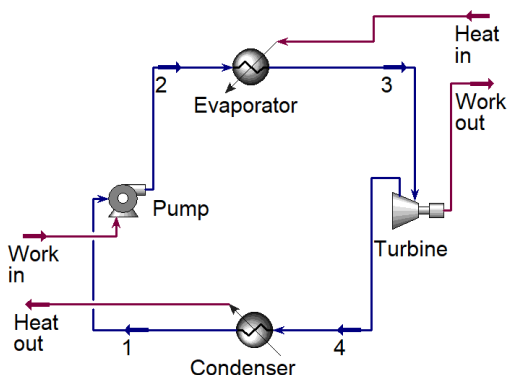
Figure 2.3: Screenshot of the base model made in Hysys.

Equation of state: In addition to a schematic of the cycle, Hysys requires an equation of state to perform simulation. The *Peng-Robinson* [4] equation of state is chosen as it popular, less computationally expensive, and already implemented in Hysys. It retains sufficient accuracy when performing calculations on hydrocarbons and mixtures of hydrocarbons compared to other models, which was first presented by Peng & Robinson [4] and later summarized by for instance Lopez-Echeverry *et al.* [15]. The relations for a binary mixture writes:

$$p = \frac{RT}{V - b_m} - \frac{a_m}{V^2 + 2b_m V - b_m^2} \tag{2.3}$$

$$a_m = \sum_{i=1}^{2} \sum_{j=1}^{2} x_i x_j (1 - k_{ij}) \sqrt{a_i a_j}, \quad b_m = \sum_{i_1}^{2} x_i b_i \tag{2.4}$$

$$a_i = 0.45724 \cdot \frac{R^2 T_{c,i}^2}{p_{c,i}} (1 + \kappa_i \cdot (1 - T_{r,i}^{\frac{1}{2}}))^2, \quad T_{r,i} = \frac{T}{T_{c,i}}, \quad b_i = 0.07780 \cdot \frac{RT_{c,i}}{p_{c,i}} \tag{2.5}$$

$$\kappa_i = 0.37464 + 1.54226 \cdot \omega_i - 0.26992 \cdot \omega_i^2 \tag{2.6}$$

where k_{ij} is the binary interaction parameter, and ω is the acentric factor. These values are found in literature and are listed in Hysys for the various substances. Subscripts i, j are indices for substances i and j, while m means mixture, and is not an index.

2.3 Inleak model

Allowing air into an organic Rankine cycle will, as indicated initially in this section, have a major impact on the cycle. To investigate how for example the pressure on the low-pressure side evolves with the amount of air present, the base model must be modified to deal with the challenges caused by using a mixture of air and hydrocarbon as working fluid. There are two major challenges that will influence the model:

Phase transition: Air and hydrocarbons have different evaporation temperatures and ambient conditions, and they can be in different phases. Working fluid can evaporate before entering the evaporator. The mixture of air and working fluid in vapor phase on the low-pressure side is the *gas phase*.

Two-phase pumping: A pump designed for pumping liquids may face issues when gas is present in the pump, reducing the efficiency and consequently flow rate. Too low flow rate may bring the cycle to halt. Furthermore, the two phases may separate inside the pump and clog it.

2.3.1 Inleak model assumptions

The inleak model will have specific conditions applied to it. This is done to automate computation and lessen workload required to compute properties. One of the assumptions that greatly simplifies computation is phase equilibrium in State 1, finding the phase composition at pump inlet would be far more challenging without this. In reality this assumption may not be the case, and a possible consequence of simplifying things is loss of accuracy. This is subject to discussion in Section 4.4.2. Core assumptions are:

Air inleak: Air is made up of 21% O_2 and 79% N_2. Air can enter at all locations in the cycle where working fluid pressure is below atmospheric pressure. This corresponds to between the turbine and the pump, between State 4 and 1 in Fig. 2.1. The model takes a fixed amount of air as input and evaluates properties for this quantity of air. No transient approaches are used, except for combustion processes. The inleak stops when the pressure of the gas phase on the low-pressure side has been raised to ambient pressure.

The air and working fluid mixture: Air and working fluid mixes isothermally, and a two-phase mixture is formed. The liquid phase is at all times composed of working fluid only. The gas phase is an ideal gas mixture of air and working fluid. At State 1, the working fluid is in phase equilibrium, this is between condenser outlet and pump inlet. The gas phase mixture is modeled as an ideal gas mixture. At State 3, the mixture is gas phase only, this is between evaporator outlet and turbine inlet. The mixture does not react until a spark or other heat sources ignites it.

2.3.2 Inleak model operation in Hysys

Hysys is able to handle mixing air and working fluid, and it is straightforward to make an inleak model in the Hysys environment. A mixing operation is added to the layout in Fig. 2.3, leading to the schematic presented in Fig. 2.4. Hysys will now calculate properties of the air and working fluid mixture and use that mixture as the new "working fluid". The mixture is pumped to high pressure, evaporated to gas phase and expanded in the turbine. If no reactions occur in the turbine, the mixture proceeds to the condenser and pump inlet. Before entering the pump a second time, the mixture will pass the inleak location, picking up more air.

In the Hysys model, the stream *WF in* represents the working fluid stream before air has leaked in. As it mixes with air and proceed through the cycle, it returns to the mixing operation as *New WF in*. The new stream is not connected to the mixing operation because a quasi-steady simulation is done, meaning that the mole fractions are not to be changed, as would happen when *New WF in* returns to the mixing.
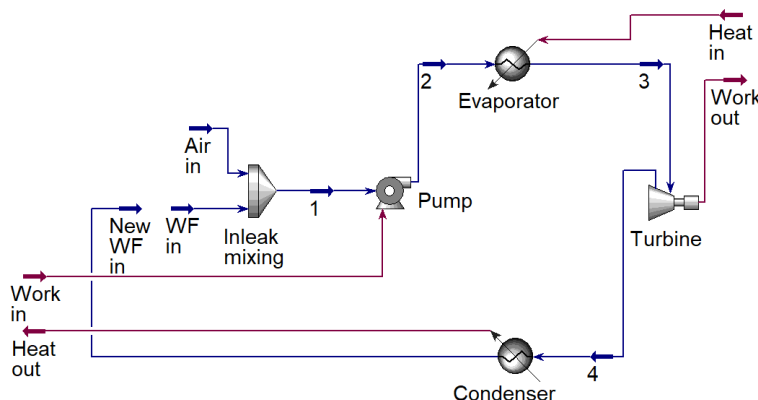
Figure 2.4: Screenshot of the inleak model made in Hysys.

Using a commercial software does carry a rather significant disadvantage; the user has no way of confirming which equations and relations the program is using. Very limited research exists on simulating air in organic Rankine cycles, thus is there no available research to support results from a commercial software. As no physical experiments are associated with this study, there is no way of doing a validation of the Hysys model. One can only trust that results from the simulations are correct.

A proposed measure to this uncertainty is expanding the mathematical base model to an inleak model with additional equations and relations, with no input from Hysys other than base states. The aforementioned challenges must be dealt with by introducing equations for phase equilibrium and specific conditions for the pump model. Results from this model will then be compared to the Hysys model, and a conclusion will be drawn regarding model reliability.

2.4   Phase transition model

To deal with the first of the two major challenges presented in Section 2.3 a phase transition model is developed. Air in gas phase and working fluid in liquid phase mixed together will produce a two-phase mixture. With a gas phase present, the working fluid will evaporate until a phase equilibrium is reached. A core assumption is that no working fluid exists as vapor phase in the air inside the breach at the moment of inleak, and the air will be saturated with working fluid just before it arrives at the pump. In other words, the working fluid will reach phase equilibrium at State 1. The flow rate of gas phase in the pump has a major impact on operating characteristics of the pump, this is discussed in Section 2.5. Thus, the estimation of the molar fractions in the gas phase must be accurate.

2.4.1   Flow evolution

Obviously, the flow will undergo a change as air leaks in. The mass flow rate of working fluid remains unchanged as it proceeds from single-phase to two-phase, this is expressed:

$$\dot{m}_{WF_0} = \dot{m}_{WF_{lq}} + \dot{m}_{WF_v} \tag{2.7}$$

where subscript 0 denotes initial state in the base model, liquid phase, and subscripts lq and v denotes liquid and vapor states, respectively, in the inleak model, all corresponding to the flow at State 1 in Fig. 2.1. This can be translated to molar flow rate by expanding with molar masses:

$$\dot{n}_{WF_0} = \dot{n}_{WF_{lq}} + \dot{n}_{WF_v} \tag{2.8}$$

since the same molar mass appear in all terms. The molar flow rate of liquid phase may be expressed as the initial molar flow rate prior to air inleak minus the molar flow rate of evaporated working fluid.

Fig. 2.5 provides a cross sectional view of the flow at State 1 just before inleak occurs (left) and a possible flow at State 1 while inleak occurs (right), at quasi-steady state. The right hand side illustration indicates that gas phase lies on top of the liquid phase. This may or may not be the case, depending on where air leaks in. The cross sectional distribution of gas phase is important at the pump inlet. This will be discussed further in the pump model.
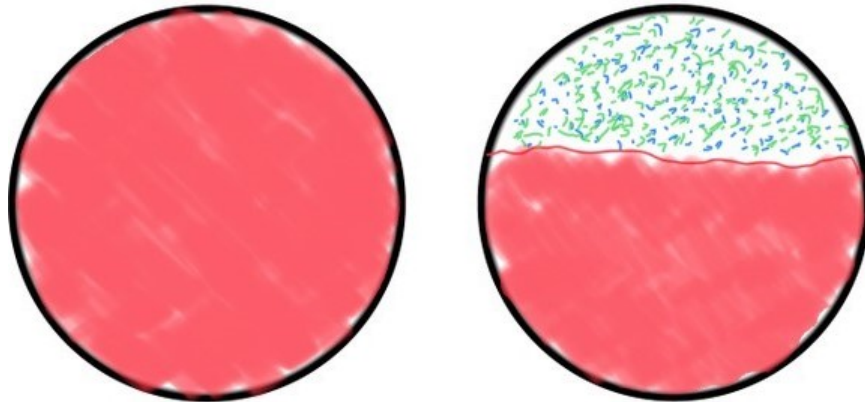

Figure 2.5: Evolution of flow in the pipe before (left) and after (right) air inleak. Red is working fluid in liquid phase, blue dots are working fluid in vapor phase, and green dots represents air.

2.4.2 Phase equilibrium for fluids

To evaluate the gas phase the partial pressure of the working fluid in vapor phase is needed. This is found from a phase equilibrium analysis where it is assumed that only the working fluid undergoes phase transition, for the sake of simplified equations. The procedure to evaluate properties at phase equilibrium is taken from Pages 785-787 in [3]. The *Clapeyron equation* writes:

$$\frac{dp_{sat}}{dT} = \frac{1}{T}\frac{\bar{h}_{lq} - \bar{h}_v}{\bar{v}_{lq} - \bar{v}_v} \tag{2.9}$$

where h is enthalpy and v is specific volume. At a given temperature, it is possible to calculate the vapor pressure at phase equilibrium through an iterative approach. The liquid properties are fixed due to the pressure and temperature being known, while the pressure is unknown for the vapor properties.

Computational method: Eq. 2.9 is solved with a numerical scheme trying to match the right- and left hand side. Following the procedure in the code shown by Fig. 2.6, the temperature is discretizised from 280 K up to the critical temperature with a step size $dT = 10^{-3}$ K. The saturation pressure is evaluated for every temperature, and a gradient is made with the built-in function *gradient*. The temperature is known, thus is the left hand side of Eq. 2.9 computed, along with the liquid properties.

```
8       %find saturation pressure gradient
9       %dT = 1e-3;
10 -    T_max = refpropm('T','C',0,'',0,substance);
11 -    T_range = 280:dT:T_max-0.1;
12 -    parfor i = 1:length(T_range)
13 -        p_sat(i) = refpropm('P','T',T_range(i),'Q',0,substance);
14 -    end
15 -    dp_satdT = gradient(p_sat,T_range);
16
17      %calculate liquid state in Clapeyron equation
18 -    index = find(abs(T_range-T)<1e-6);
19 -    dpdT = dp_satdT(index);
20 -    h_lq = refpropm('H','T',T,'P',p_lq,substance);
21 -    v_lq = 1/refpropm('D','T',T,'P',p_lq,substance);
```

Figure 2.6: Screenshot of Matlab code using the Clapeyron equation.

Note that the command *parfor* is a for-loop where paralleled processing is enabled to speed up computation. The command *refpropm* calls thermodynamic from *Reference Fluid Thermodynamic and Transport Properties Database*, commonly abbreviated REFPROP [16]. REFPROP is both a standalone software for computing thermodynamic data but also offers integration with Matlab to solve equations, the integration is performed through the file *refpropm.m* written by Keith Wait *et al.* [17].

The vapor properties on the right hand side is computed according to the procedure in the code shown by Fig. 2.7. In short the code is computing enthalpy and specific volume for many values of vapor pressure, and then comparing left and right hand sides. The array p_v contains all values of vapor pressure to evaluate, and is limited by the floor value (rounded down to closes integer) of the saturation pressure and the saturation pressure plus ten times the step size. Preliminary calculations found this interval to be appropriate, as the vapor pressure will be close to saturation pressure. p_{v_0} is the saturation pressure.

```
24          %define pressure range for vapor state
25          %dp = 1e-5;
26  -       p_v_0 = refpropm('P','T',T,'Q',0,substance);
27  -       p_v = floor(p_v_0):dp:p_v_0+10*dp;
28
29          %calculate vapor state in Clapeyron equation for all possible pressures
30  -    ⊟parfor i = 1:length(p_v)
31  -           h_v(i) = refpropm('H','T',T,'P',p_v(i),substance);
32  -           v_v(i) = 1/refpropm('D','T',T,'P',p_v(i),substance);
33  -     end
34
35          %determine which vapor pressure to obtain from the equation
36  -       rhs = dpdT*1e+3;
37  -       lhs = (1/T)*((h_v-h_lq)./(v_v-v_lq));
38  -       error = rhs-lhs;
39  -       index_p = find(abs(error)==min(abs(error)));
```

Figure 2.7: Screenshot of Matlab code using the Clapeyron equation.

The computational method is brute force, but computing with a pressure step size $dp = 10^{-6}$ kPa requires 10 minutes of computing and yields an error of order 10^{-5}, this is affordable as it is performed only once for each working fluid.

2.4.3 Main input parameter

A suitable input parameter of the inleak model is how much air is present in the cycle. It was initially assumed that adding air will cause a certain amount of working fluid to evaporate, this amount must be expressed as a function of amount of air present. The amount of air will also influence combustion properties, of course, which is to be discussed in Section 3.

Gas Volume Fraction: Commonly abbreviated GVF, this property is important when evaluating the pump performance. By dividing the volumetric flow rate of gas phase by the total volumetric flow rate a fraction is found. For this cycle the total volumetric flow rate is the sum of gas and liquid flow rate. Much research on multiphase flow is done with GVF as a variable.

$$GVF = \frac{\dot{Q}_{gas\ phase}}{\dot{Q}_{total}} = \frac{\dot{Q}_{gas\ phase}}{\dot{Q}_{gas\ phase} + \dot{Q}_{liquid\ phase}} \tag{2.10}$$

GVF($\dot{n}_{air}$): It is desired to have the molar flow rate of air, $\dot{n}_{air}$, as an input parameter. This flow rate is the molar flow rate of air inside the pipes, which is constant if used as an input parameter. Thus, an expression for the function GVF($\dot{n}_{air}$) is sought. The starting point is the definition of GVF and a relation between flow rates, $\dot{Q} = \dot{m}/\rho = M\dot{n}/\rho$, is used:

$$GVF = \frac{\dot{m}_{gas}/\rho_{gas}}{\dot{m}_{gas}/\rho_{gas} + \dot{m}_{liquid}/\rho_{liquid}} = \frac{M_g\dot{n}_g/\rho_g}{M_g\dot{n}_g/\rho_g + M_{lq}\dot{n}_{lq}/\rho_{lq}} = \frac{M_g\dot{n}_g}{M_g\dot{n}_g + M_{lq}\dot{n}_{lq}\rho_g/\rho_{lq}} \tag{2.11}$$

where the subscripts have been shortened. The relation between volumetric and molar flow rate was used in Eq. 2.11 and the equations was multiplied by gas density ρ_g. The gas phase is composed of air and working fluid in vapor phase, and the liquid phase is composed of working fluid only. The molar flow rate of gas is split into molar flow rates of air and working fluid:

$$\dot{n}_g = \dot{n}_{air} + \dot{n}_{WF_v} \tag{2.12}$$

13

This relation is used in Eq. 2.11 along with the expression for liquid molar flow rate found in Eq. 2.8 since the liquid phase only consists of working fluid:

$$GVF = \frac{M_g(\dot{n}_{air} + \dot{n}_{WF_v})}{M_g(\dot{n}_{air} + \dot{n}_{WF_v}) + M_{lq}(\dot{n}_{WF_0} - \dot{n}_{WF_v})\rho_g/\rho_{lq}} \tag{2.13}$$

Next, the molar flow rate of evaporated working fluid must be related to the molar flow rate of air. For this purpose the humidity ratio ω is used:

$$\frac{\dot{m}_{WF_v}}{\dot{m}_{air}} = \omega = \frac{M_{WF_v}p_{WF_v}}{M_{air}p_{air}} \tag{2.14}$$

where pressure p_{WF_v} the partial pressure of working fluid in the gas phase, found from the Clapeyron equation. p_{air} is the partial pressure of air in the gas phase, which can be expressed as the pressure of the gas phase on the low-pressure side minus partial pressure of working fluid, $p_{air} = p_{gas} - p_{WF_v}$. An expression for p_{air} is to be found. This expression can be translated to a molar basis using the molecular weights:

$$\frac{\dot{n}_{WF_v}M_{WF_v}}{\dot{n}_{air}M_{air}} = \frac{\dot{m}_{WF_v}}{\dot{m}_{air}} = \frac{M_{WF_v}p_{WF_v}}{M_{air}p_{air}} \implies \frac{\dot{n}_{WF_v}}{\dot{n}_{air}} = \frac{p_{WF_v}}{p_{air}} = \frac{p_{WF_v}}{p_{gas} - p_{WF_v}} \tag{2.15}$$

The molar fraction of working fluid in vapor state is related to the molar fraction of air through the vapor- and ambient pressure. Note that the ratio of molar flow rates is constant, hence are the molar fractions in the gas phase independent of $\dot{n}_{air}$. The found expressions for molar flow rates are inserted in Eq. 2.11:

$$GVF(\dot{n}_{air}) = \frac{M_g(\dot{n}_{air} + \dot{n}_{air}\frac{p_{WF_v}}{p_{gas} - p_{WF_v}})}{M_g(\dot{n}_{air} + \dot{n}_{air}\frac{p_{WF_v}}{p_{gas} - p_{WF_v}}) + M_{lq}(\dot{n}_{WF_0} - \dot{n}_{air}\frac{p_{WF_v}}{p_{gas} - p_{WF_v}})\rho_g/\rho_{lq}} \tag{2.16}$$

The molar flow rate of working fluid before inleak, $\dot{n}_{WF_0}$, remains in the equation. This value is a design parameter and not much of interest, but intuitively it is obvious that a higher molar flow rate of a liquid demands a higher molar flow rate of gas for the gas volume fraction to scale properly. The expression for GVF will rather use a normalized flow rate of air, namely $\dot{n}_{air}/\dot{n}_{WF_0}$. Eq. 2.16 is divided by $\dot{n}_{WF_0}$ and simplified:

$$GVF(\frac{\dot{n}_{air}}{\dot{n}_{WF_0}}, p_{gas}) = \frac{M_g(1 + \frac{p_{WF_v}}{p_{gas} - p_{WF_v}})\frac{\dot{n}_{air}}{\dot{n}_{WF_0}}}{M_g(1 + \frac{p_{WF_v}}{p_{gas} - p_{WF_v}})\frac{\dot{n}_{air}}{\dot{n}_{WF_0}} + M_{lq}(1 - \frac{\dot{n}_{air}}{\dot{n}_{WF_0}}\frac{p_{WF_v}}{p_{gas} - p_{WF_v}})\rho_g/\rho_{lq}} \tag{2.17}$$

where vapor pressure is found from Eq. 2.9. Gas and liquid phase densities are set by temperature and pressure of the respective phases, with values found by calling the function refpropm presented in the previous section. Gas and liquid phase molar masses are set by molar fractions in both phases. Eq. 2.17 relies on the assumption of phase equilibrium at State 1 and is therefore only valid between condenser outlet and pump inlet. The pressure of the gas phase, p_{gas}, is also an input parameter, an attempt to relate it to $\dot{n}_{air}$ is to be done in Section 2.6.

Maximum flow rate of air: It is hypothesised that at a certain value of $\dot{n}_{air}/\dot{n}_{WF_0}$ the cycle will stop, the pump is unable to drive the flow. A literature review on multiphase pumping may reveal a certain operating range for multiphase pumps in terms of GVF, this operating range can be translated to the ratio of molar flow rates. If there are no hard limits a range of ratios is used. The gas volume fraction is to be plot against the ratio of molar flows in the results.

2.5   Pump model

The pump is a vital part of the cycle as explained in the section introducing the inleak model. Based on experience it is known that the pump will struggle as more air is introduced. A literature review is done with several goals in mind. The first is to gain knowledge of typical pumps appropriate for small-scale organic Rankine cycles. The second goal to investigate how these pumps operate when exposed to different fluids. The third is to investigate which mechanisms cause pumps to struggle when gas phase is introduced. A final, but optional, goal is to find a limit for the gas volume fraction.

2.5.1   Literature review, pumps in organic Rankine cycles

Chapter 18 of [2] provides brief descriptions of small-scale organic Rankine cycles and what equipment is commonly used. One of the main references in this chapter is the doctoral thesis of Bernard Aoun from 2008 [6]. Aoun investigates suitability of equipment found on the accessible market for cycles of smaller scale ($\sim$ 3kW). Part of this investigation is performed on pumps, and Aoun finds positive displacement pumps to perform much better than centrifugal pumps, due to their ability to build high pressure with lower flow rates. Especially reciprocating piston- and diaphragm pumps are well-suited as these can handle fluids with low viscosity (below 0.4 mPa $\cdot$ s) [6].

Another major reference in the very same chapter is the doctoral thesis of Stefano Clemente from 2013 [7]. Clemente revisits the results of Aoun and argues that gear pumps are also suited for fluids of low viscosity if lubricant is added to the working fluid, creating a solution with sufficiently high viscosity. An experiment with a gear pump in a cycle with a mixture of R245fa and lubricant oil is performed, with the oil being 15-20 % of the mixture on a mass-basis. Clemente finds that a mixture with average kinematic viscosity below 5 mm^2/s will drastically decrease the performance of that specific gear pump [7]. Fig. 2.8 from the doctoral thesis reports how kinematic viscosity ν influences volumetric flow rate and pressure change.
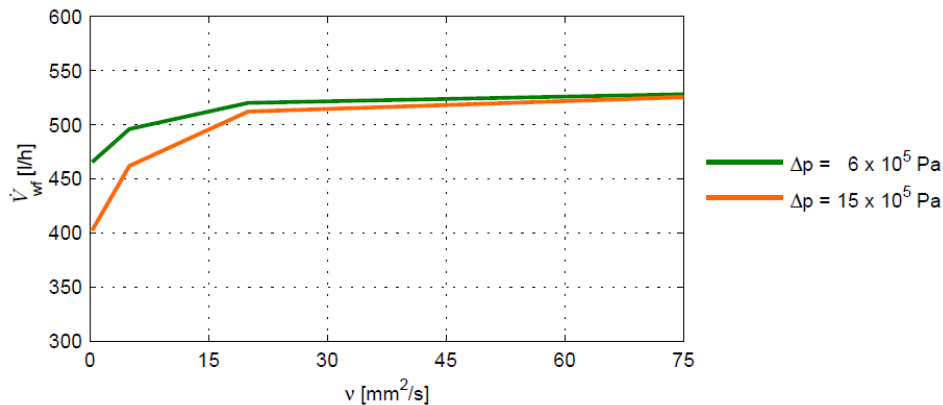
Figure 2.8: Volumetric flow rate plot against kinematic viscosity, figure from [7].

Observe how reducing the kinematic viscosity to a certain range of values causes at first a gradual but the a more sudden drop in volumetric flow rate. Increasing the pressure change over the pump causes a further drop in volumetric flow rate as more fluid is pushed backwards. This is also observed in Fig. 2.9. The pump can handle increased pressure difference while maintaining the flow rate, but at $\nu = 5$ mm^2/s there are major changes.

Figure 2.9: Volumetric flow rate plot against pressure increase over the pump, figure from [7].

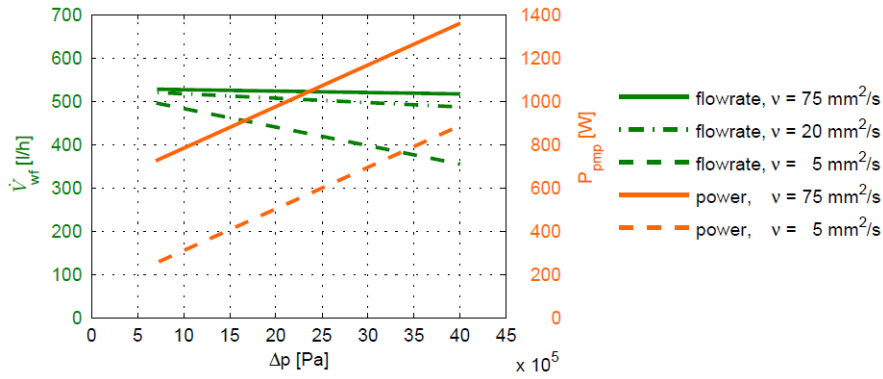The conclusion of both Aoun and Clemente is that working fluids with too low viscosity is a challenge for positive displacement pumps as they have insufficient lubricating properties. Clemente finds that backflow, leakage, and surge are consequences of insufficient lubrication in gear pumps, these lower volumetric flow rate and pressure ratio.

2.5.2   Literature review, multiphase flow in pumps

The doctoral thesis of Alberto Serena from 2016 [8] performs an experimental study on a centrifugal pump where air is injected into the water to be pumped upstream of the pump. Pump operation with multiphase flow (MP) is compared to operation with single phase flow (SP) at the same operating points, the comparison is done with the parameter $f_\psi = P_{MP}/P_{SP}$, where P head delivered by the pump. Serena finds through experiments that reducing volumetric flow rate, reducing rotational speed, and increasing gas volume fraction causes the pump to "clog", its performance drops to nil [8]. It is observed in Figs. 2.10 and 2.11 that performance gradually reduces when the relative flow rate q^*, which is the actual volumetric flow rate divided by a reference flow rate at design conditions, is unity, but reducing the flow rate causes a more sudden drop in performance. The rotational speed has great influence on where this drop occurs with respect to GVF, there is no absolute limit for the gas volume fraction. The performance ratio f_ψ exceeds unity at for some conditions, but this is not of interest.
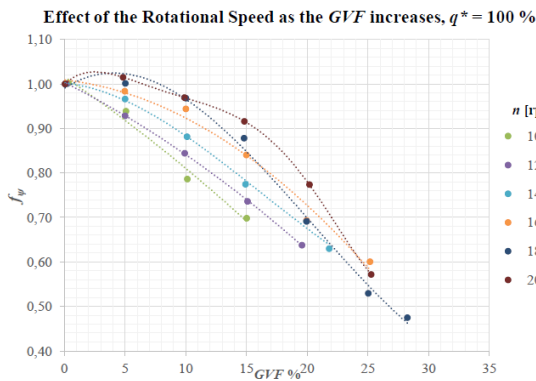

Figure 2.10: Performance plot against GVF for volumetric flow rate equal to 100% of nominal flow rate, figure from [8].
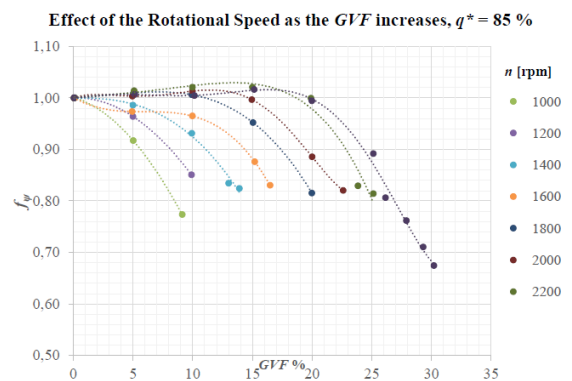

Figure 2.11: Performance plot against GVF for volumetric flow rate equal to 85% of nominal flow rate, figure from [8].

The doctoral thesis [8] also includes images from a high-speed for flow visualization. Serena observes visually that the gas phase separates from the liquid phase and forms recirculating pockets on the pressure side of the blades. From this observation he concludes that these pockets appear at certain operating points, and as parameters q^* and rotational speed decreases and GVF increases, the pocket can grow in size. This is illustrated in Fig. 2.12 where a drop in performance is caused by gas pockets of increasing size.
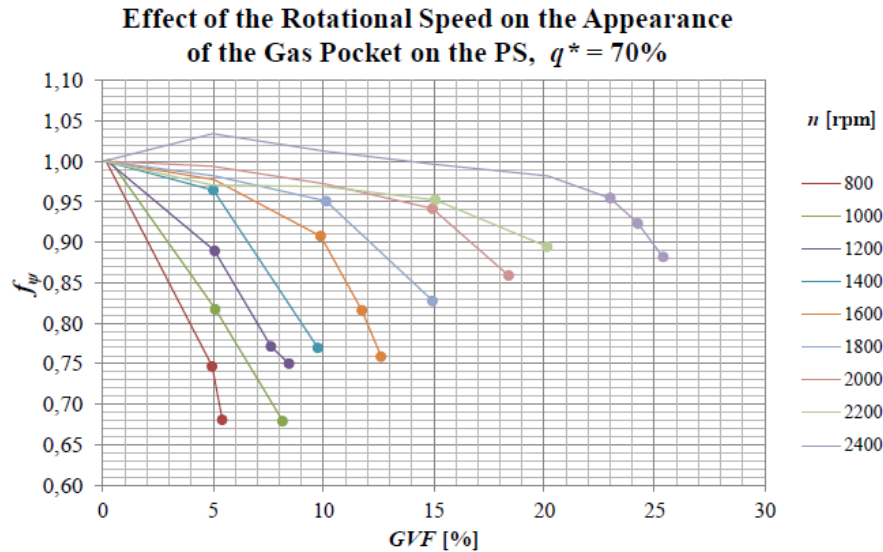

Figure 2.12: Performance plot against GVF for volumetric flow rate equal to 70% of nominal flow rate. Observe how the curves progresses from horizontal to vertical over a short span of GVF. Figure from [8].

Serena concludes that certain mechanisms are responsible for the drop in performance. Gas pockets unable to separate from the blades but preventing liquid to pass is one of them. Gas pockets can also force the flow to deflect and enter at less favorable angles, in addition to blocking the flow that was originally supposed to enter at that location, the blocked flow may flow back to where it came from, causing a surging phenomena. This is rather unstable.

2.5.3   Physical pump model and two-phase mechanisms

From the literature review on pumps in organic Rankine cycles, and especially the doctoral thesis of Clemente [7], it is evident that gear pumps are well suited. The working principle of a gear pump is cutting of a volume of fluid and displacing it between two gears to from the inlet to the outlet. To achieve this, the clearance between moving gear and stationary parts must be very low for fluid not to leak from outlet to inlet side/flow backwards. Viscous fluids have a hard time passing through tight clearances compared to fluids with low viscosity. This is why pump manufacturers specify a certain range for viscosity of the working fluid, for instance within 3 - 75 mm^2/s in [7]. Aoun [6] classifies low-viscous fluids as those with dynamic viscosity $\mu < 0.4$ mPa.s.

This thesis will assume a gear pump is used as part of the investigation on subatmospheric organic Rankine cycle. The gear pump is to be exposed to two-phase flows and two major mechanisms from the three doctoral theses are used [6][7][8]:

Viscosity and lubrication: Fig. 2.13 from [7] illustrates the gear pump used in the study. Fluid is trapped between the teeth of the gears. The gears rotate while the crescent shape between them is stationary. Fluids with a viscosity below a specified range can flow through the clearances between the crescent shape and the gears, effectively causing back flow and leakage, as discussed by [7].
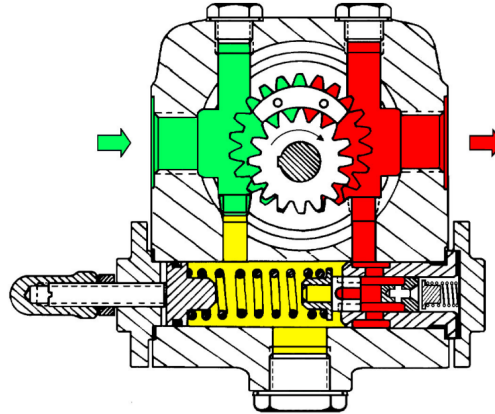

Figure 2.13: Schematic of the gear pump investigated by Clemente, figure from [7].

It is assumed that the gas phase consisting of air and working fluid in vapor phase has sufficiently low viscosity to pass through the clearances while the liquid phase cannot, liquid phase will rather lubricate the gears. The pressure difference over the pump is assumed large enough to force the gas phase back through the clearances. The amount of gas flowing backwards is unknown, but it is assumed to not affect the pressure of the high-pressure side of the pump.

Gas pockets: Serena [8] in his doctoral thesis found several unsteady mechanisms causing issues in centrifugal pumps, among them is phase separation and pockets of gas phase blocking the flow. If only gas phase were to migrate from high-pressure side to low-pressure side through the aforementioned clearances between rotating and stationary surfaces, something like a phase separation could indeed occur.

With the assumption that only gas phase slips through the clearances there is a risk of it accumulating on the inlet side, as there are no other ways for the gas phase to travel. [8] found certain limits for GVF for that specific pump, these may not be imposed on the gear pump as these are two different machines. However, various values for the GVF can be simulated to find a relation to the combustion properties.

2.6 Numerical inleak model

The numerical inleak model is result of the effort made in Sections 2.3 through 2.5 to make a mathematical model independent of Hysys. The phase transition model outlined a way to estimate the molar fractions of the gas phase, this enabled estimation of the gas volume fraction. Based on a literature survey on components in organic Rankine cycles a gear pump was chosen and evaluated for two-phase flow. The survey found that fluids of low viscosity can slip through clearances and cause back flow in the pump. Moreover, the survey found a possibility for low viscosity fluid to accumulate and block the flow at pump inlet. From these findings it is hypothesised that sufficient amounts of gas phase can indeed bring the cycle to halt.

2.6.1 Distribution of air in an organic Rankine cycle

If gas phase can slip through clearances in the pump there is reason to believe that the amount of air is far higher on the low-pressure side compared to high-pressure side. Thus, the mixture of air and working fluid will differ greatly from one side to another. To be able to perform numerical computation it is assumed that the amount of gas on the high-pressure side was brought there by being solved in the liquid, and that only the solubility of air is of interest, since the other part of the gas phase is the same substance as the liquid. This may bring an underestimation of the molar fractions on high-pressure side as it is possible that some gas phase can proceed through the pump without leaking back through the clearances, however, quantifying this for a specific pump requires experiments on that specific machine, which is beyond the scope of study.

Solubility of air in working fluids: Battino *et al.* [18] performs a study of nitrogen solved in various hydrocarbon fluids where n-alkanes and benzene are of interest. Air gas is different from nitrogen, but only data on solubility of nitrogen in liquids were obtained in the study, hence are the equations for nitrogen solubility used for the gas phase. One argument supporting this assumption is that nitrogen gas accounts for a large portion of air, and the values obtained from equations proposed by [18] are used to estimate an order of magnitude, rather than exact values. Regardless, the study will lose accuracy, this is to be discussed in Section 4.4.2. Eqs. 2.18 and 2.19 may compute solubility of N_2 in n-alkanes and benzene. The equations are valid in the temperature and pressure ranges relevant to this study. Working fluids with evaporation pressures far below atmospheric pressure may not be evaluated with these equations.

$$\ln(\chi_1) = -12.882 + 12.268/\tau + 4.4131 \cdot \ln(\tau) + 1.0098 \cdot \ln(P) - 0.062824 \cdot C \qquad (2.18)$$

$$\ln(\chi_1) = -7.4974 + 1.9422 \cdot \ln(\tau) - 0.0061750 \cdot P + 0.97481 \cdot \ln(P) \qquad (2.19)$$

where P is partial pressure of air in the gas phase in MPa, τ is temperature in 100 K and C is number of carbon atoms in the n-alkane. The equations are plot in Figs. 2.14 and 2.15.
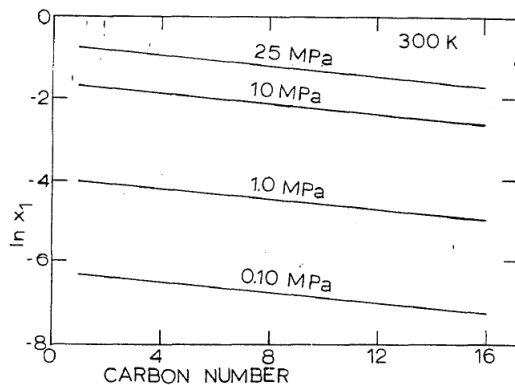

Figure 2.14: Molar fraction solubility of nitrogen in the n-alkanes at $p = 1$ atm. as a function of carbon number, figure from [18].
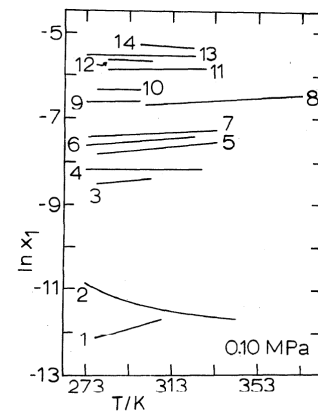

Figure 2.15: Some representative mole fraction solubilities of nitrogen at $p = 1$ atm. Curve 5 displays nitrogen solubility in benzene, figure from [18].

[18] states that χ_1 is the mole fraction at specified pressure. It is interpreted as how much air can possibly be solved in the liquid working fluid. In other words, a fraction χ_1 multiplied with liquid flow rate will be molar flow rate of air solved in liquid. This contradicts the assumption made when expressing GVF in Section 2.4.3 as it was assumed that liquid flow only consists of working fluid in liquid phase. However, for n-pentane at 1 atm., 300 K, $\chi_1 \approx 10^{-3}$, which yields a negligible flow rate if inserted in Eq. 2.11. The following section, where results are presented, will comment this further.

2.6.2 Cycle properties evolving with air inleak

The main cycle properties of interest when regarding air inleak in this study, are molar fractions of air on high-pressure and low-pressure sides, as well as pressure evolution on the low-pressure side. Temperatures are assumed to remain constant as the mixing is isothermal. Section 2.4.3 found that the ratio of molar flow rates, $\dot{n}_{air}/\dot{n}_{WF_0}$, and gas phase pressure on low-pressure side, p_{gas}, are appropriate free variables.

Low-pressure side: The molar fraction of air in the gas phase on the low-pressure side is expressed as a function of the molar flow rates that makes up the gas phase:

$$x_{air_{LP}} = \frac{\dot{n}_{air}}{\dot{n}_{air} + \dot{n}_{WF_v}} = \frac{p_{gas} - p_{WF_v}}{p_{gas}} \tag{2.20}$$

where vapor- and gas pressure comes from the humidity relation presented when developing Eq. 2.17. Note that this presumes phase equilibrium, which is only assumed between condenser outlet and pump inlet. The pressure of the gas phase is defined for the interval:

$$p_{WF_v} < p_{gas} < p_{amb} \tag{2.21}$$

where the condition $p_{WF_v} < p_{gas}$ comes from the fact that some air must be present for the working fluid to evaporate. The upper limit is imposed as an inleak situation is to be evaluated, and no inleak occurs if the pressure is ambient or above. Recall that the gas pressure is the total pressure of the gas phase, and that the partial pressure of the working fluid is set, meaning that only air pressure will increase as more air enters the cycle. Thus, the air pressure must be within the following interval:

$$0 < p_{air} < p_{amb} - p_{WF_v} \tag{2.22}$$

Working fluids with saturation pressure close to ambient will greatly reduce the maximum air partial pressure in the cycle. Unfortunately, as it was not possible to relate p_{gas} and $\dot{n}_{air}/\dot{n}_{WF_0}$, it is not possible to find a limit for the ratio of molar flow rates based on the ambient pressure. The limit for this parameter may be found from the investigation performed on pumps in Section 2.5, namely from a GVF-limit, as this ratio is present in the expression for the gas volume fraction.

High-pressure side: It is assumed that only the liquid phase plus the air solved in the liquid is able to proceed to the high-pressure side. Molar fractions are evaluated at State 3/turbine inlet where it is assumed that all flows are in vapor phase. The molar flow rate on this side of the cycle is expressed:

$$\dot{n}_{HP} = \dot{n}_{lq} + \dot{n}_{air,lq} = \dot{n}_{lq}(1 + \chi_1) \tag{2.23}$$

where both free variables, $\dot{n}_{air}/\dot{n}_{WF_0}$ and p_{gas} appears. One of these would preferably be a function of the other, but after a quick look at the ideal gas law, $pV = n\bar{R}T$, one may realize that three out of four properties must be known (excluding $\bar{R}$ which is constant), and that the volume is in this case unknown. χ_1 is found from Eqs. 2.18 and 2.19. This value accounts in the stream of air solved in liquid working fluid.

Flow rate $\dot{n}_{lq}$ is the molar flow rate of liquid working fluid in Eq. 2.8. It is desired to normalize $\dot{n}_{HP}$ by $\dot{n}_{WF_0}$ such that further derivation is similar to the methods used in Section 2.4.3 when developing Eq. 2.17:

$$\frac{\dot{n}_{HP}}{\dot{n}_{WF_0}} = \frac{(\dot{n}_{WF_0} - \dot{n}_{WF_v})(1 + \chi_1)}{\dot{n}_{WF_0}} = (1 - \frac{\dot{n}_{air}}{\dot{n}_{WF_0}} \frac{p_{WF_v}}{p_{gas} - p_{WF_v}})(1 + \chi_1) \tag{2.24}$$

A few observations are made from this relation. Eq. 2.24 reveals that molar flow rate on high-pressure side increases as p_{gas} increase, but decreases as $\dot{n}_{air}/\dot{n}_{WF_0}$ increase. In addition, χ_1 increases with p_{gas} as this increases air partial pressure, [18] finds that solubility increases with pressure, as can be observed in for example Eq. 2.18. The physical interpretation of this is that a larger volume of air can be solved in the same volume of liquid, but the volume of liquid is reduced due to more evaporation. Finally, the molar fraction of air at State 3/turbine inlet is expressed from molar flow rates:

$$x_{air_{HP}} = \frac{\dot{n}_{air,lq}}{\dot{n}_{lq} + \dot{n}_{air,lq}} = \frac{\dot{n}_{lq}\chi_1}{\dot{n}_{lq} + \dot{n}_{lq}\chi_1} = \frac{\chi_1}{1 + \chi_1} \tag{2.25}$$

where it is observed that the molar fraction of air on the high-pressure side only varies with solubility χ_1. Working fluid in vapor phase is the other substance besides air at this state, $x_{WF_{HP}} = 1 - x_{air_{HP}}$. To compute the molar fraction of air on the high-pressure side, the values found from Eqs. 2.18 and 2.19 are used. Air is solved into the liquid working fluid before pump inlet, at State 1 in Fig. 2.1 the liquid is saturated with air. Solubility is evaluated at the pump inlet where temperature is 30°C and pressure is calculated from $p_{air} = p_{gas} - p_{WF_v}$. Pressure on the high-pressure side was assumed to be constant at all times when developing the pump model, with the reasoning that only an experimental study on a specific pump could provide a proper model for outlet pressure for that pump.

2.7 Results, cycle modeling

Results corresponding to the steps illustrated in Fig. 2.2 are presented. The previous sections have developed methods to compute a range of properties relevant to the cycle.

Working fluid: Two working fluids are suggested based on the discussion on desired working fluid properties, namely n-pentane (n-C5H12) and benzene (C6H6). These have significantly different saturation pressures at 30°C. This will provide information on how organic Rankine cycles with operating pressure close to ambient and far below ambient differs when exposed to air.

Thermodynamic states: The states with unknown properties (mainly temperature) are calculated from the Hysys base model, assuming isentropic efficiency of pump and turbine to be 80% and no pressure drops in heat exchangers. Table 2.1 reports thermodynamic states.

Table 2.1: Organic Rankine cycle state properties calculated from Hysys base model.

Working fluid	Property	State 1	State 2	State 3	State 4	Thermal efficiency
n-Pentane	Temperature [°C]	30.00	30.82	150.00	83.79	15.7%
	Pressure [bar]	0.820	15.0	15.0	0.820	
Benzene	Temperature [°C]	30.00	30.24	150.00	61.89	17.7%
	Pressure [bar]	0.159	5.8	5.8	0.159	

2.7.1 Hysys inleak model

Simulations performed in the Hysys environment took the molar fraction of air in the gas phase as input, and reported cycle efficiency and mixture properties at State 1 in Fig. 2.1. Figs. 2.16 and 2.17 are plots of mixing temperature and cycle efficiency varying with the molar fraction of gas present in the gas phase, equal to the molar fraction in Eq. 2.20. Both simulations are done with up to its limit set by $p_{gas} \rightarrow p_{amb}$, see Fig. 2.18 for numerical values. Due to the difference in vapor pressure the benzene simulation is performed on a wider range of $x_{air_{LP}}$. Observe how the temperature and efficiency drops as soon as air is introduced, and that this is the case for both working fluids. The simulation using benzene is able to reach the point where the efficiency is zero, the energy input in the pump is equal to the energy generated by the turbine. It is observed that the efficiency turned negative beyond $x_{air_{LP}} \approx 0.4$, this is set to zero as negative efficiency is not of interest.
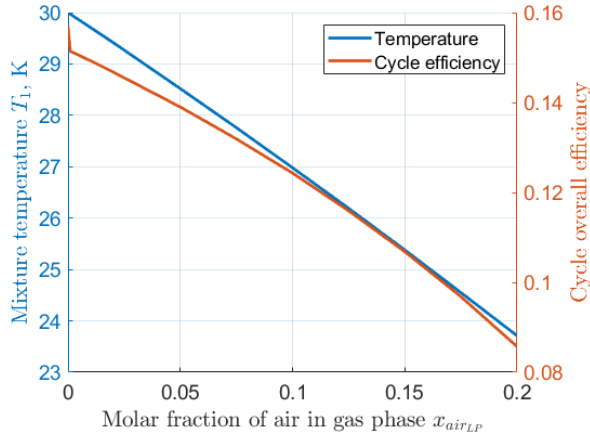
Figure 2.16: Hysys inleak model results with n-pentane as working fluid.
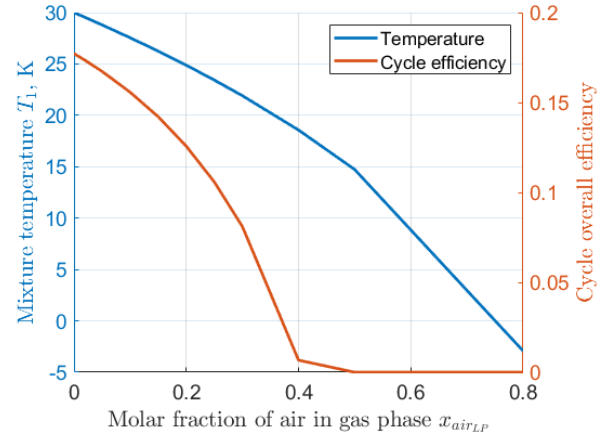
Figure 2.17: Hysys inleak model results with benzene as working fluid.

Non-isothermal mixing: For the simulation with benzene as working fluid, the temperature drops below zero degrees Celsius. The trend of decreasing temperature with increasing $x_{air_{LP}}$ has also been observed when simulating the Hysys inleak model with water as working fluid at appropriate condensation and evaporation pressures. Intuitively, this is incorrect as there would be no way the temperature would drop that much by just mixing air and water. This will be discussed in Section 4.4.1.

2.7.2 Numerical inleak model

Air molar fractions: Following the approach described in Section 2.4.2 and Eq. 2.9, the vapor pressure of working fluid at phase equilibrium is estimated. Calculations find that this pressure is very close to the saturation pressure at that temperature. For n-pentane: $p_{WF_v} = 0.8199$ bar, for benzene: $p_{WF_v} = 0.1592$ bar, at a temperature of 30°C. The vapor pressures are significantly different, according to Eq. 2.21 the interval for the gas phase pressure on low-pressure side, p_{gas}. Using this pressure as the free variable, the molar fraction of air in the gas phase on both pressure sides of the cycle is estimated from Eqs. 2.20 and 2.25, where solubility was estimated using Eqs. 2.18 and 2.19. Fig. 2.18 is a plot of the molar fraction of air varying with the gas phase pressure between condenser outlet and pump inlet:
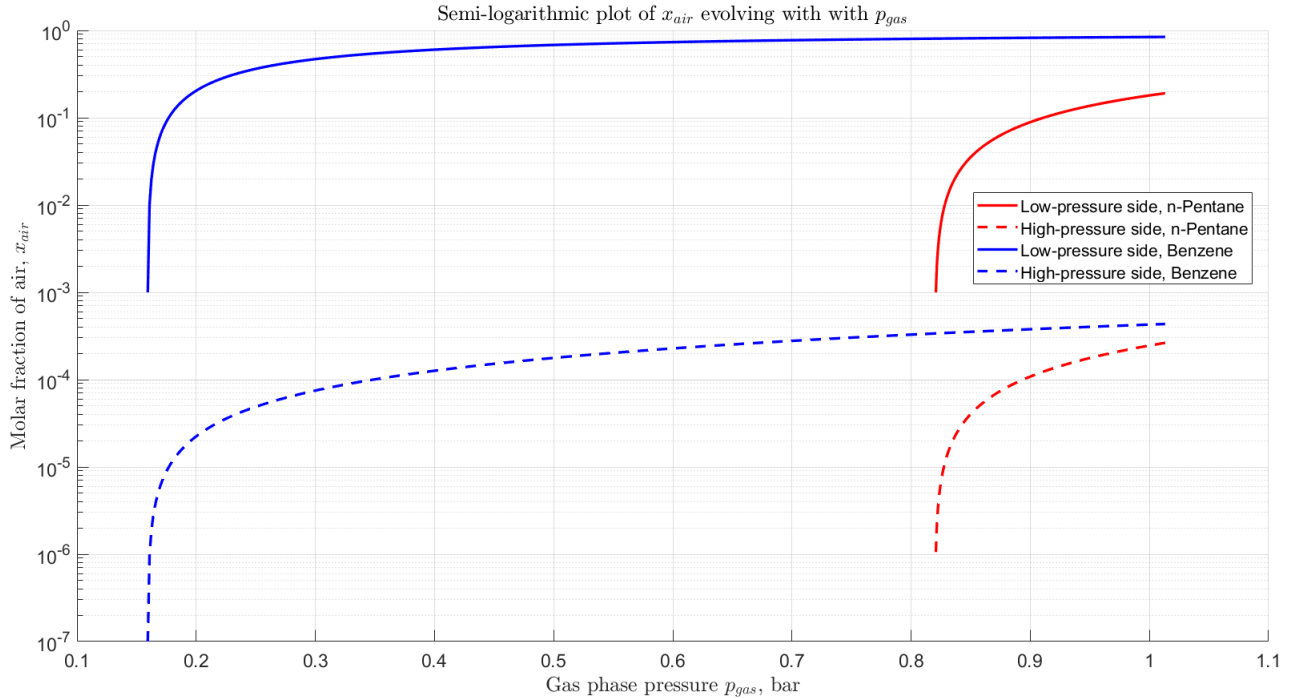

Figure 2.18: Molar fraction of air as function of gas phase pressure.

The curves in Fig. 2.18 reveal that molar fraction of air on the high-pressure side is on a far lower scale than on the low-pressure side. In addition, the molar fraction of air in the benzene-cycle (blue) is higher than in the n-pentane-cycle (red) on the low-pressure side due to the lower vapor pressure p_{WF_v}, yet the curves are much closer on the high-pressure side. Furthermore, the benzene curves grow rapidly while the n-pentane curves are slower. Finally, all molar fractions are far higher as $p_{gas} \rightarrow p_{amb}$, which is to be expected.

Molar flow rate on high-pressure side: Figs. 2.19 and 2.20 are iso-contours of the molar flow rate on the high-pressure side formulated by Eq. 2.24. The value of $\dot{n}_{HP}/\dot{n}_{WF_0}$ is constant along each line, where the value is found from the color bars displayed in the figures. The molar flow rate of air on the low-pressure side normalized by total molar flow rate of working fluid, $\dot{n}_{air}/\dot{n}_{WF_0}$, is now an input parameter in addition to gas phase pressure on the low-pressure side. The figures reveal that an increase in molar flow rate of air causes less of the original flow $\dot{n}_{WF_0}$ to progress through the pump and to the high-pressure side, this is caused by more and more working fluid being evaporated and blocked from passing through the pump.

An interesting observation is that increasing gas phase pressure will for both fluids increase $\dot{n}_{HP}/\dot{n}_{WF_0}$ if $\dot{n}_{air}/\dot{n}_{WF_0}$ is kept constant. A possible explanation is that solubility increases with pressure as shown in Fig. 2.14, but this effect is rather minor. When revisiting Eq. 2.24 it becomes evident that increasing gas phase pressure will increase the size of the first bracket, causing an increase in flow rate on the high-pressure side.

Gas volume fraction: Lastly, the plots of the gas volume fraction, Figs. 2.21 and 2.22 are evaluated. The variables remain unchanged from the two previous plots but the coloring inverts, causing the highest values of GVF to appear on top. The initial observation is that increasing $\dot{n}_{air}/\dot{n}_{WF_0}$ leads to an increase in GVF, this is intuitive. What is rather counter-intuitive is that increasing gas phase pressure causes a decrease in GVF when keeping $\dot{n}_{air}/\dot{n}_{WF_0}$ constant, much like what was observed in Figs. 2.19 and 2.20. A possible explanation for this is that the term $\frac{p_{WF_v}}{p_{gas}-p_{WF_v}}$ appearing in Eq. 2.17 decreases as gas phase pressure increases.

Figs. 2.10 to 2.12 all operates with a GVF up to 30%. This would correspond to the blue, dark blue, and purple contour lines in Figs. 2.21 and 2.22. A limit for the gas volume fraction was discussed after the literature review in Section 2.5.2, this limit indicated that gas pockets could form at the pump inlet and completely block the inflow. If a limit for the gas volume fraction is set to be 0.3, and the gas phase pressure is allowed to take any value, then this means that the parameter $\dot{n}_{air}/\dot{n}_{WF_0}$ must be limited, and that this limit varies with p_{gas}. In Fig. 2.21 the third contour line from the bottom is the GVF = 0.3-line. If the fraction cannot cross this line, that means that the ratio must be in the interval $\dot{n}_{air}/\dot{n}_{WF_0} \in [10^{-5}, 10^{-3}]$. The lowest values of the interval are from values of p_{gas} close to p_{WF_v}, where a singularity occurs, higher values of p_{gas} allows $\dot{n}_{air}/\dot{n}_{WF_0}$ to increase up to 10^{-3}. This interval is nothing more than a crude estimate as it is impossible to know the exact limit for GVF without experimenting on a physical pump.

The influence of gas phase pressure: Figs. 2.19 to 2.22 all show that increasing gas phase pressure on the low-pressure side, p_{gas}, allows for higher values of the ratio of molar flow rates, $\dot{n}_{air}/\dot{n}_{WF_0}$, if $\dot{n}_{HP}/\dot{n}_{WF_0}$ or GVF are kept constant. The physical interpretation of this is that the amount of air passing through a cross section, $\dot{n}_{air}$, takes up less area in that cross section if the pressure is increased, as if it was compressed. Thus, if the amount of area occupied by molar flow rate of air is to remain constant under increasing gas phase pressure, then the flow rate must increase. This may seem counter intuitive as a higher gas phase pressure means more air present in the cycle, it may indicate that the p_{gas} and $\dot{n}_{air}/\dot{n}_{WF_0}$ are in fact not independent, but somehow related.
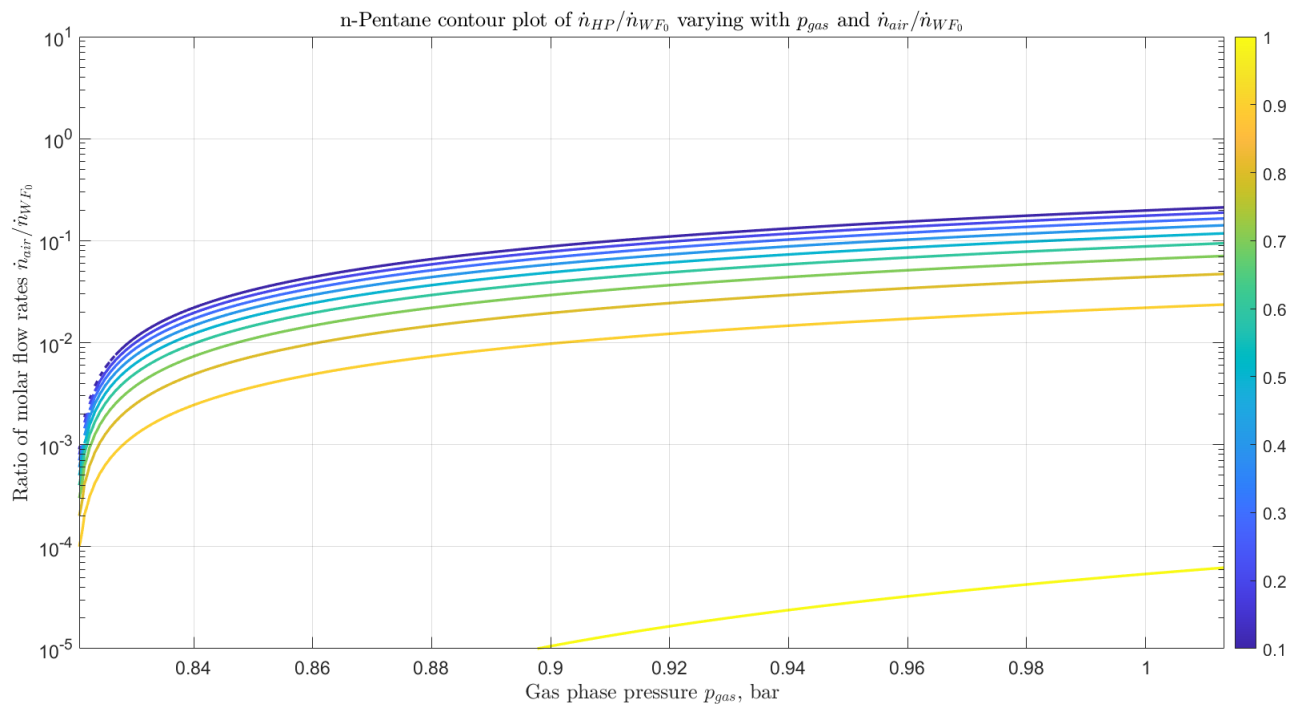
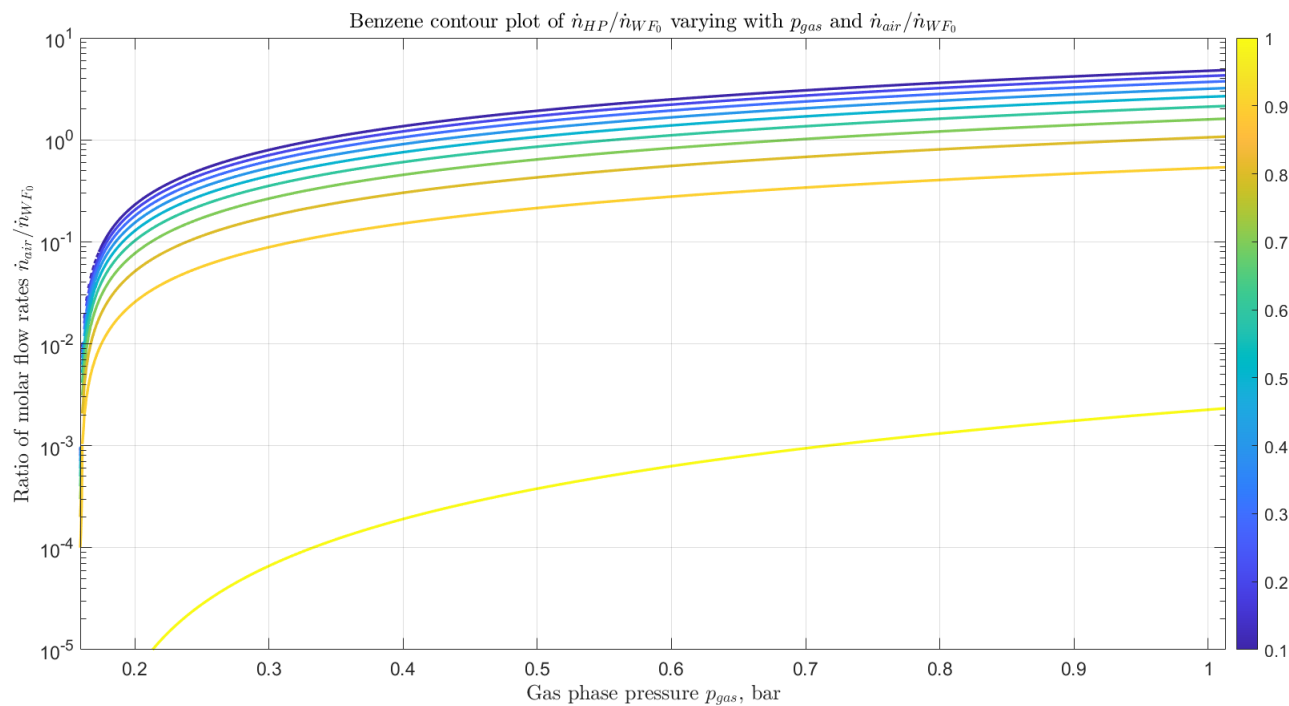Figure 2.19: Evolution of molar flow rate on high-pressure side in the n-pentane cycle.

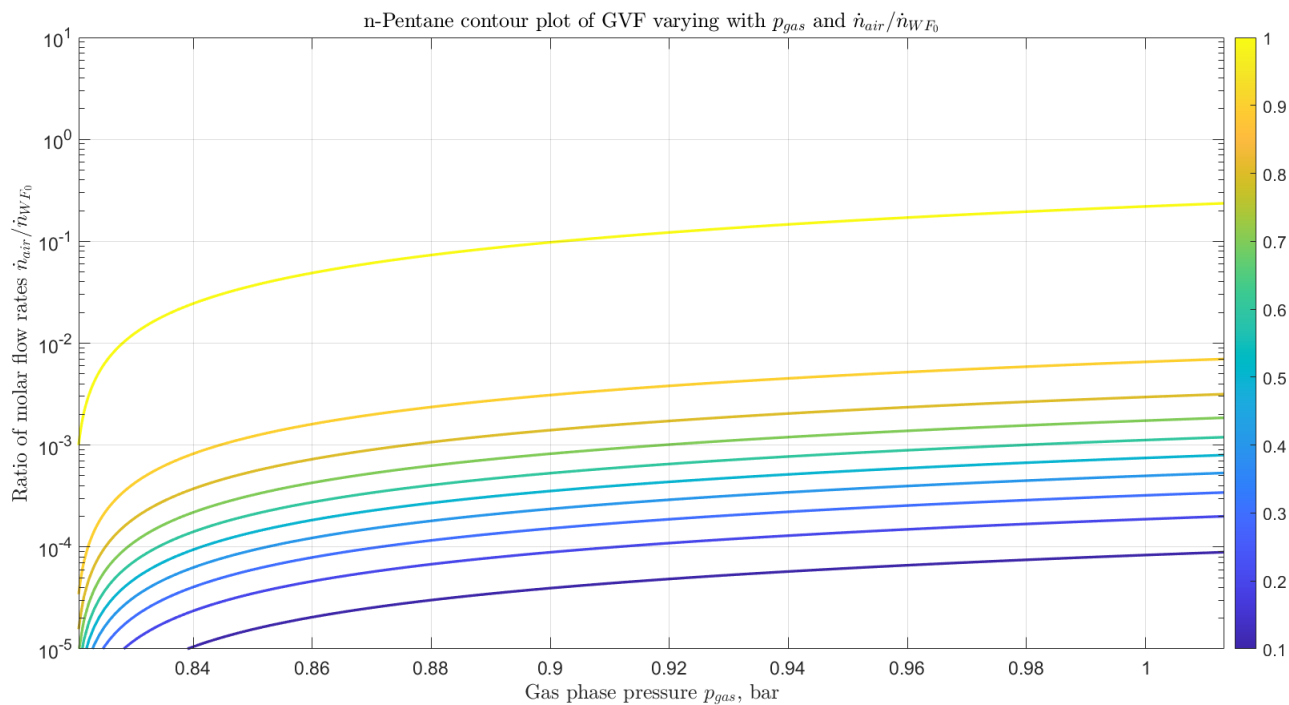Figure 2.20: Evolution of molar flow rate on high-pressure side in the benzene cycle.

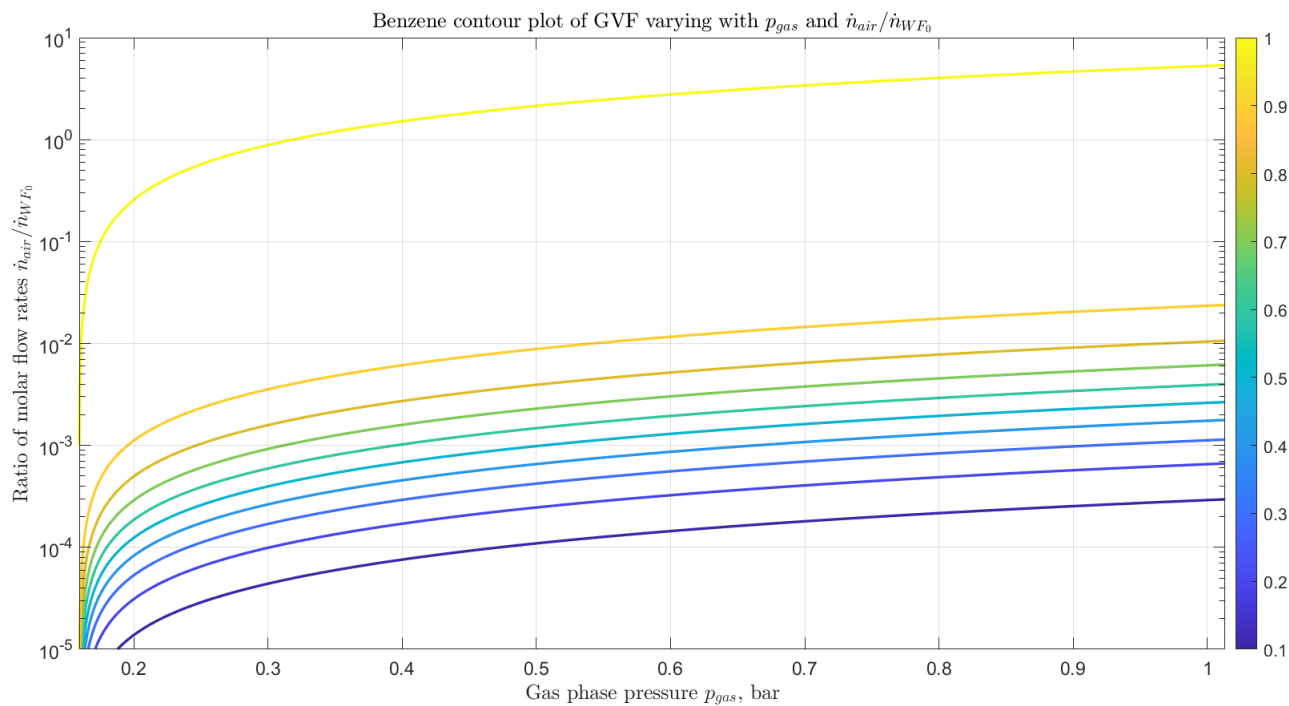Figure 2.21: Evolution of gas volume fraction in the n-pentane cycle.

Figure 2.22: Evolution of gas volume fraction in the benzene cycle.

COMBUSTION ANALYSIS

Air leaking into the system brings two challenges. The first was discussed in the previous chapter. The second is that the hydrocarbon based working fluid and air mixes and creates a combustible mixture, and this mixture may ignite if sparks are present. This section will discuss how chemical reactions in combustion occur, what it takes for a premixed flow to ignite and form a self-sustaining flame, and how the combustion properties vary as more air is added. Numerical solving in Cantera is also presented.

3.1 What is combustion?

Combustion is a process where fuel undergoes rapid oxidation at high temperatures. It is presumed that this concept is familiar to the reader, but for convenience the following terms are repeated and notation presented. Global reaction for combustion of methane:

$$CH_4 + 2O_2 \rightarrow CO_2 + 2H_2O \tag{3.1}$$

Elementary reaction for decomposition of methane:

$$CH_4 + O \rightarrow CH_3 + OH \tag{3.2}$$

A kinetic mechanism is a proposed scheme of how specific molecules react with each other and contains numerical values related to the reactions, in essence it contains a series of elementary reactions. One example of a kinetic mechanism for methane is illustrated in Fig. 3.1, developed by Qi et $al.$ [19]. For more information on important mechanisms for fuel decomposition the reader is referred to Chapter 5 of [9].

3.1.1 Roadmap

With the general concepts in combustion modeling revisited it is time to outline the approach used in this study. A complete reactive flow model is to be developed and subjected to the two most relevant fields in combustion regarding organic Rankine cycles; ignition and flame structures. The models are simulated using Matlab and the results are to be evaluated in terms of risk and consequences of combustion. Fig. 3.2 illustrates how equations and conditions are sewn together to a reactive flow model, the flow model is then simulated with different numerical schemes depending on whether ignition or flames are to be evaluated.
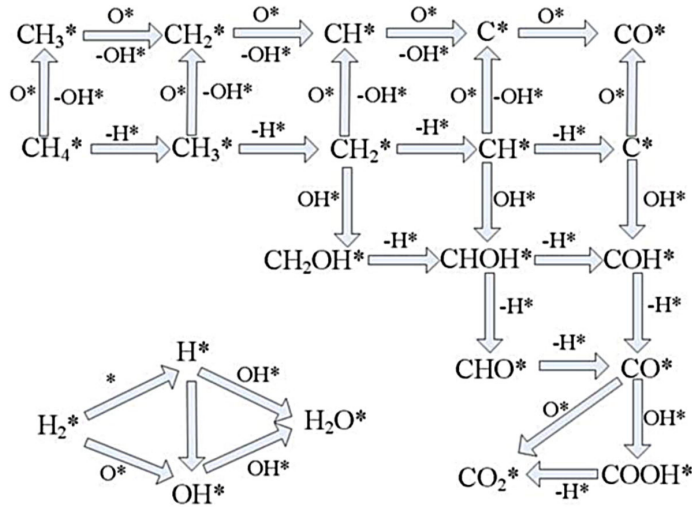
Figure 3.1: Possible oxidation of methane leading to water and carbon dioxide, figure from [19].
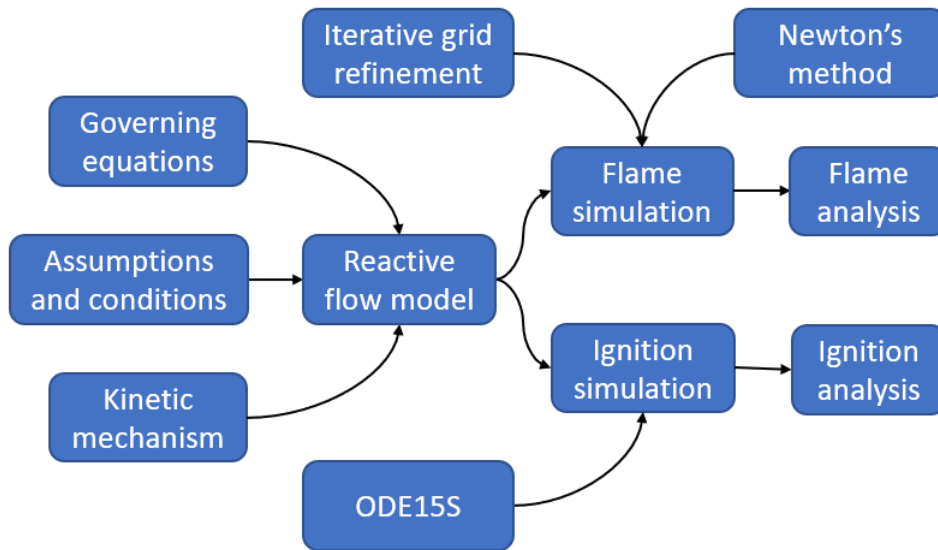
Figure 3.2: Roadmap of the reacting flow methodology.

3.1.2 Reaction properties

Each chemical reaction in a kinetic mechanism is associated with certain numerical values. These values describe the possibility of that specific reaction to occur, and relate to the rate at which a type of molecule is produced or consumed/destroyed, which is quantified as the net production rate. This would be the sum of all reactions producing type of molecule, minus the sum of all reactions consuming that molecule:

$$\frac{\text{Change in concentration of molecule}}{\text{Change in time}} = \sum \text{Producing reactions} - \sum \text{Consuming reactions} \quad (3.3)$$

If a kinetic mechanism consisted of reaction 3.2 and the reverse/opposite reaction was possible, the rate at which methane is consumed would be expressed:

$$\frac{d[\text{CH}_4]}{dt} = -k_f \cdot [\text{CH}_4][\text{O}] + k_r \cdot [\text{CH}_3][\text{OH}] \tag{3.4}$$

where $[\text{CH}_4]$ is the volumetric concentration of methane in kmol/m^3 and k_f, k_r are forward and reverse *rate coefficients*, respectively. The forward reaction consumes methane while the reverse reaction produces methane. The rate coefficients are determined by the numerical values mentioned earlier through the modified Arrhenius equation (cite):

$$k(T) = AT^b \cdot exp(\frac{-E_A}{RT}) \tag{3.5}$$

where A, b, E_A are numerical values found in reaction mechanisms. The physical interpretation of these quantities can be found in Chapter 4 of [9]. It is evident that the rate coefficients may be highly temperature dependent for a large value for b. Formulating chemical reactions and experimentally determining these numerical values is subject to modern research. As one may realize, having kinetic mechanisms with many species and reactions will increase computational effort as Eqs. 3.4 and 3.5 must be formulated for all species, and the equations may include several producing or consuming reactions.

3.2 Reactive flow model

The flow in the organic Rankine cycle is now regarded as reactive. It was assumed initially that the flow was non-reactive before all fluid streams are evaporated and the flow is gas phase only. Observations in the results from the non-reactive models indicated that the gas phase on the low-pressure side may also be combustible as it consists of working fluid and air. In other words, combustion is to be evaluated for States 1 and 3 in Fig. 2.1. The mixture of working fluid and air at both states may cause exothermic chemical reactions to happen. This calls for a new model as properties like temperature, velocity, mass fractions and density may change due to said reactions.

3.2.1 Assumptions and conditions

With many properties no longer being constant there may be variation in all possible dimensions. To ease the burden of computation the flow is assumed one dimensional, major changes will occur in the direction of travel/along pipe central axis rather than from wall to wall. Ignition is modeled transient rather than spatial and is caused by sparks only. Any flames appearing are steady. There is no propagation of flames upstream/flashback. Pressure is constant for all combustion processes, this is to be shown in the flame methodology. The gas mixture of air and working fluid is regarded as a homogeneous mixture prior to combustion.

Boundary conditions: The second law of thermodynamics is the main boundary condition for this reacting flow. At the boundary all fuel or all oxidizer is spent and no further reactions can occur spontaneously. Reacting flow will at one point reach equilibrium, at this point the temperature T and mass fraction Y_i of substance i are constant, the derivatives with respect to dimension x_1, which can be distance or time, are zero at the end boundary. As the simulations are one dimensional only these boundary conditions are sufficient to close the equations.

$$\frac{dT}{dx_1}\bigg|_{x_1=\infty} = 0, \quad \frac{dY_i}{dx_1}\bigg|_{x_1=\infty} = 0 \tag{3.6}$$

Initial conditions: Before any reactions occur the flow has certain properties fixed by the inleak model. Temperature and base pressure are listed in Table 2.1 in Section 2.7. Molar fractions are set by the equations developed for the inleak model in Section 2.6.2. The fractions are functions of the pressure of the gas phase on the low-pressure side, which is set to be a free variable. The initial conditions are:

$$T_0 = T(x_1 = 0), \quad Y_{i_0} = Y_i(x_1 = 0) \tag{3.7}$$

3.2.2 Equivalence ratio Φ

A central property related to combustion, representing how much oxidizer is present in the flow. The current fuel/oxidizer ratio divided by the stoichiometric fuel/oxidizer ratio, abbreviated with the Greek letter Φ. The stoichiometric ratio is set for different hydrocarbons. A Φ much higher than unity indicates that there is more fuel than what can be burned with the available oxidizer, and that much fuel will still remain after combustion. Eq. 3.8 states that the fuel is a stream of working fluid (not yet related to any streams in the cycle) and the oxidizer is a stream of oxygen gas. Observe that Φ must have a different expression for low-pressure and high-pressure side due to the phase separation in the pump.

$$\Phi = \frac{\dot{n}_F/\dot{n}_{Ox}}{(\dot{n}_F/\dot{n}_{Ox})_{st}} = \frac{\dot{n}_{WF}/\dot{n}_{O_2}}{R_{st}} \tag{3.8}$$

Low-pressure side: Regarding the flow in the pipes at the low-pressure side it is obvious that the gas phase is a mixture of working fluid and oxygen. The streams in Eq. 3.8 must be the stream of working fluid in vapor phase, $\dot{n}_{WF_v}$, and the stream of oxygen from the air leaking in:

$$\Phi_{LP} = \frac{\dot{n}_{WF}/\dot{n}_{O_2}}{R_{st}} = \frac{\dot{n}_{WF_v}/\dot{n}_{O_2}}{R_{st}} \tag{3.9}$$

Since the composition of air is assumed to be 21% O_2 and 79% N_2 the molar flow rate of oxygen gas can be expressed from the molar flow rate of air into the system:

$$\dot{n}_{air} = \dot{n}_{O_2} + \dot{n}_{N_2} = \dot{n}_{O_2} + 3.762 \cdot \dot{n}_{O_2} = 4.762 \cdot \dot{n}_{O_2} \implies \dot{n}_{O_2} = \dot{n}_{air}/4.762 \tag{3.10}$$

This is used along with the relation between molar flow rates and partial pressure found from the humidity ratio expression when deriving Eq. 2.17:

$$\Phi_{LP} = \frac{\dot{n}_{WF_v}/\dot{n}_{O_2}}{R_{st}} = 4.762 \cdot \frac{\dot{n}_{WF_v}/\dot{n}_{air}}{R_{st}} = \frac{4.762}{R_{st}} \cdot \frac{p_{WF_v}}{p_{gas} - p_{WF_v}} \tag{3.11}$$

The equivalence ratio for the low-pressure side, Φ_{LP}, takes the inverse shape of Eq. 2.20. Section 2.6.2 stated that p_{gas} has a maximum value at ambient pressure, meaning that there is a lower limit to Φ_{LP}. This limit is hereby referred to as the Φ-limit or limit for equivalence ratio, and is widely used in the results section. This limit is of especially of interest as it often is value of Φ closest to unity.

High-pressure side: Section 2.6.1 found that only flow in liquid phase is pumped to the high-pressure side. Furthermore, it is assumed that combustion will not occur until all flows are evaporated, forming a single-phase flow. In that case the streams in Eq. 3.8 must be stream of working fluid passing through the pump and the stream of oxygen solved in the liquid. When assuming gas phase only the molar fractions yields the flow rates. Using Eqs. 2.24 and 2.25:

$$\Phi_{HP} = \frac{\dot{n}_{HP}x_{WF_{HP}}/\dot{n}_{HP}x_{O_{2HP}}}{R_{st}} = \frac{4.762}{R_{st}} \cdot \frac{x_{WF_{HP}}}{x_{air_{HP}}} \tag{3.12}$$

$$\Phi_{HP} = \frac{4.762}{R_{st}} \cdot \frac{1}{x_1} = \left(\frac{1}{x_1} \cdot \frac{p_{gas} - p_{WF_v}}{p_{WF_v}}\right) \cdot \Phi_{LP} \tag{3.13}$$

Eq. 3.13 reveals that the equivalence ratio on the high-pressure side is only varying with the solubility of air in liquid working fluid and that it is always higher than Φ_{LP}. The condition on the low-pressure side will change as air enters, meaning that the solubility will rise as a consequence of higher pressure, as seen in for example the solubility chart of N_2 in n-alkane, Fig. 2.18. Thus, Φ_{HP} will decrease as solubility increases, meaning that more air is present on the high-pressure side. Like Φ_{LP}, Φ_{HP} must also have a limit as $p_{gas} \rightarrow p_{amb}$. Observe how both Φ_{LP} and Φ_{HP} increases as gas phase pressure on low-pressure side increases.

3.2.3 Literature review, kinetic mechanisms

A kinetic mechanism is required to evaluate how reactants are consumed and products produced. Which kinetic mechanism to choose depends on the working fluid, temperature range and whether soot formation is to be considered or not. Due to time limitations this study will consider a model without soot or NO_x formation as these will add increased complexity to the mechanism in the form of additional species and reactions.

GRIMECH 3.0 A common kinetic mechanism that is thoroughly discussed in Chapter 5 of [9] is the GRI-Mech 3.0 kinetic mechanism developed by Smith *et al.* [20]. It consists of 53 species and 328 reactions, with alkanes up to propane. The mechanism is also integrated as a part of the toolbox Cantera which is to be presented later this section. It is not applicable in this study as neither n-pentane nor benzene are included in the list of species.

CRECK modeling group: *The Chemical Reaction Engineering and Chemical Kinetics Lab*, abbreviated CRECK, is a research group at *Politechnico di Milano* conducting research and development of kinetic mechanisms. The homepage [12] provides an overview of previous research on kinetic mechanisms with several detailed and semi-detailed kinetic mechanisms available for download. One of the listed detailed kinetic mechanisms that are of relevance is the *Toluene Primary Reference Fuels (TPRF) HT + LT + Alcohols mechanism (Version 2003, March 2020)*, developed by the research group and further revised by Ranzi *et al.* [21][22] and Bagheri *et al.* [23]. The first publication investigates the need for confirming the core kinetic mechanism $C_0 - C_4$ which is present in many reduced kinetic mechanisms. The second evaluates previously neglected reaction classes for combustion at temperatures near 600 K, and finds that these are significant at this value. The last publication performs validation of the current mechanism with a large quantity of experimental data. It finds that the mechanism shows good predictive capabilities when evaluating combustion of methane.

The kinetic mechanism is chosen based on the results from these three publications where the applicability of the mechanism was confirmed for low-temperature combustion, which is expected when Φ is far from unity. Both n-pentane and benzene are included as major reactants, meaning they have several possible ways to break down as seen in Fig. 3.1. The kinetic mechanism includes 339 species and 9781 reactions, which could potentially cause long runtime for simulations.

3.2.4 Cantera

Cantera [11] is an open-source toolbox compatible with programming languages like Matlab. The main reason for using Cantera as part of this analysis is that it can create and modify gas objects, as well as being compatible with detailed kinetic mechanisms. The possible species and reactions for this gas object is determined by the chosen kinetic mechanism, it serves as an input parameter. When the gas object is created and its intensive properties set (temperature, pressure, and mass fractions) certain operations can be performed on the object. These operations include reporting extensive properties, finding the equilibrium state, and reporting the net production rate presented in Eq. 3.4. One of the goals in this study is to evaluate how the gas phase in the organic Rankine cycle changes as it undergoes ignition, or how the properties of the gas phase changes over the length of a flame. The main properties of interest are temperature and mass fractions. Two different operations are performed with Cantera, ignition and flame structure.

Cantera is installed on a computer running Windows with both Matlab and Python/Visual Studio Code interface. Less demanding operations like ignition simulations and simple flame simulations with simplified kinetic mechanisms are performed with the Matlab interface. Complex operations like flame simulations with equivalence ratios much different from unity and detailed kinetic mechanisms are performed with the Python interface. This choice was based on initial calculations where it was found that the Python interface performed calculations faster. Matlab is used for simpler calculations simply because the author is more familiar with Matlab than Python.

Kinetic mechanisms in Cantera   Cantera has its own format for kinetic mechanisms, different from the commonly used *CHEMKIN* format. Conversion is performed through the script *ck2cti* or *ck2yaml* (new in version 2.5). The CHEMKIN format has a different file for kinetic mechanism, thermodynamic properties, and transport properties. The Cantera format combines these three into one text file, Fig. 3.3 is a screenshots of the kinetic mechanism in Cantera format:

```
species(name='H2O',
        atoms='H:2 O:1',
        thermo=(NASA([200.00, 1420.00],
                     [ 4.06061172E+00, -8.65807189E-04,  3.24409528E-06,
                      -1.80243079E-09,  3.32483293E-13, -3.02831314E+04,
                      -2.96150481E-01]),
                NASA([1420.00, 3500.00],
                     [ 2.66777075E+00,  3.05768849E-03, -9.00442411E-07,
                       1.43361552E-10, -1.00857817E-14, -2.98875645E+04,
                       6.91191131E+00])),
        transport=gas_transport(geom='nonlinear',
                                diam=2.605,
                                well_depth=572.4,
                                dipole=1.844,
                                rot_relax=4.0))
# Reaction 2
reaction('H2 + O <=> H + OH', [5.080000e+04, 2.67, 6292.0])
```

Figure 3.3: Themodynamic and transport properties, and a reaction on Cantera format.

3.3 Ignition

"For ignition to occur, an amount of energy must be added that is sufficient to raise the temperature of a slab of gas of a thickness approximately equal to the laminar flame thickness to the adiabatic flame temperature."

The ignition criterion formulated by Williams [24] describes that in order to ignite a mixture its temperature must be raised close to the adiabatic flame temperature of that mixture. In the organic Rankine cycle where air is present there is a mixture of hydrocarbon and air; both fuel and oxidizer are present. For convenience, there is only a risk of ignition if this gas mixture comes in contact with a heat source which can raise the temperature sufficiently, autoignition is left out. It is assumed that this heat source takes the form of sparks generated by rotating equipment, typically pump or turbine/expander. The spark is set to raise the temperature of a gas volume such that it ignites according the criterion formulated by Williams in [24].

3.3.1 Governing equations

An important assumption is the homogeneous gas mixture where time is assumed to be the only relevant dimension. Advection-diffusion equations are irrelevant due to independence of spatial dimensions. Reacting flow will change the mass fractions through net production rate $\dot{\omega}_i$, it is desired to relate change in properties like temperature and species mass fractions to this parameter. From Chapter 8 in [9], the transient energy and species mass concentration equations write:

$$\rho c_p \frac{dT}{dt} = \dot{q}''' = \sum_{i=1}^{N} \bar{h}_{f,i}^o(T) \cdot \dot{\omega}_i \implies \frac{dT}{dt} = \frac{1}{\rho c_p} \sum_{i=1}^{N} \bar{h}_{f,i}^o(T) \cdot \dot{\omega}_i \tag{3.14}$$

$$\frac{dY_i}{dt} = \frac{M_i \dot{\omega}_i}{\rho} \tag{3.15}$$

where $\bar{h}_{f,i}^o(T)$ is the enthalpy of formation of species i on molar basis and M_i is the molar mass of species i.

3.3.2 Numerical approach

Cantera is used to compute the production rate for all species and evaluate the gas object at each instance to compute temperature and heat release. Eqs. 3.3 and 3.4 describes how Cantera computes production rate for all species, at the current state (temperature and mass fractions) Eq. 3.3 is calculated for all species by taking all reactions into consideration. The chosen reaction mechanism includes 339 species and 9781 reactions, meaning that there may be several producing and/or consuming reactions for all species. Eq. 3.5 is computed for every reaction, and in sum this demands much computational resources.

The production rate is calculated for the current instance where temperature and mass fractions are known. To determine said properties at the next instance the differentials found from Eqs. 3.14 and 3.15 are multiplied by the time step size and added to current values. For property ψ at instance $n + 1$ this simply writes:

$$\psi_{n+1} = \psi_n + \left.\frac{d\psi}{dt}\right|_n \cdot dt_n \tag{3.16}$$

where dt_n is time step size at instance n. The size of time steps and correspondingly the instances are determined by the numerical solver, which in this case is the ordinary differential equation solver *ode15s* developed by MathWorks. Eqs. 3.14 and 3.15 forms a system of linear, ordinary differential equations which are solved by the ode15s solver. Instances are placed based on tolerances set by the user.

3.3.3   Ignition simulation

Cantera offers various example scripts, among them are *ignite_hp* and *conhp*. These have proven to have sufficiently quick runtime even with detailed kinetic mechanisms, and due to this they have been used as a base. The script conhp is the case where a reacting flow is under constant pressure and enthalpy, and is where Eqs. 3.14 and 3.15 are implemented. The script ignite_hp calls the solver ode15s with the function conhp that is to be solved, along with tolerances, time interval, and initial conditions.

ignite_hp: The main script to run when simulating ignition. Fig. 3.4 shows how the gas object is defined (here it is n-pentane) and set to an initial state in terms of temperature, pressure, and molar fractions. The initial temperature is chosen arbitrary as it is assumed that sparks can heat the gas mixture to any temperature. The equivalence ratio Φ is also chosen arbitrary, but is to be compared to what was found in Section 3.2.2. Note that the boundary conditions in Eq. 3.6 are not used here, a time interval is set in line 15.

The reasoning behind this revisits the situation where ignition can occur. A homogeneous gas volume is assumed to be heated by a spark in close proximity. If the now high-temperature gas volume does not ignite within a certain time its flow rate will bring it far away from the heat source, increasing the heat transfer to other gas volumes and/or pipe walls. The gas volume is given a time limit to ignite, after this it is assumed to lose its heat to the surroundings. The limit is set to be 10 seconds but of course, if ignition is about to occur at the time limit the limit is extended.

```
3    %Pentane: C5H12
4    pentane = Solution('chem_CRECK.cti');
5    ratio_st = 1/8;
6    t_end = 50;
7    comp = sprintf('NC5H12:1,O2:%.4f,N2:%.4f', 1/(phi*ratio_st), 3.762/(phi*ratio_st)); %determine amount of air
8
9    set(pentane,'T',temp_0,'P',1500000,'MoleFractions',comp);      %set properties of gas
10   mw = molecularWeights(pentane);                                %MW of gases
11   nsp = nSpecies(pentane);                                       %number of species
12
13   %SOLVING THE EQUATIONS
14   y0 = [temperature(pentane); massFractions(pentane)];          %initial conditions
15   tel = [0,t_end];                                              %time interval
16   options = odeset('RelTol',1.e-10,'AbsTol',1.e-10,'Stats','on'); %options for ode
17   t0 = cputime;
18   out = ode15s(@conhp,tel,y0,options,pentane,mw);               %solving the ode
19   disp(['CPU time = ' num2str(cputime - t0)]);                  %time spent
```

Figure 3.4: Screenshot of the script ignite_hp, developed by [11].

Lastly, ode15s is called to solve the system of ordinary differential equations contained in conhp. Details regarding the solver is left out of this study, see documentation by Shampine & Reichelt [25] for a complete description of the solver. Absolute and relative error tolerances are set in line 16, these causes the solver to create additional instances if the local error on the current instance exceeds the tolerances.

conhp: The system of ordinary differential equations to solve. Fig. 3.5 shows how the gas object is set to the state at the current grid point (mass fractions, temperature, and pressure), the array y contains this information. $\dot{\omega}_i$ is found for all species with the internal function $netProdRates(gas)$ integrated in Cantera, where gas is the gas object. $\dot{\omega}_i$ is used to compute dT/dt in line 10 and dY_i/dt for all species in line 18. All functions used in conhp are internal functions developed by the Cantera developers, documentation on these functions can be found at the documentation page [26]. There are no original contributions made to conhp in this study.

```matlab
1   function dydt = conhp(t, y, gas, mw) %#ok<INUSL>
2   |
3   % Set the state of the gas, based on the current solution vector.
4   setMassFractions(gas, y(2:end), 'nonorm');
5   set(gas, 'T', y(1), 'P', pressure(gas));
6   nsp = nSpecies(gas);
7
8   % energy equation
9   wdot = netProdRates(gas);
10  tdot = - temperature(gas) * gasconstant * enthalpies_RT(gas)' * wdot / (density(gas)*cp_mass(gas));
11
12  % set up column vector for dydt
13  dydt = [tdot; zeros(nsp, 1)];
14
15  % species equations
16  rrho = 1.0/density(gas);
17  for i = 1:nsp
18      dydt(i+1) = rrho*mw(i)*wdot(i);
19  end
```

Figure 3.5: Screenshot of the script conhp, developed by [11].

Ignition simulations are performed with 500°C or 1000°C as initial temperature, as well as various values for Φ, on both the low-pressure and high-pressure side of the cycle.

3.4 Flame structure

When ignition occurs, it is possible for flames to establish. A self-sustaining flame is able to heat the gas mixture entering the flame until it becomes reactive, hence the term self-sustaining. In other words, sparks are not needed for further combustion. It is desired to evaluate at which values of the equivalence ratio Φ flames are able sustain themselves, and connect these values of Φ to the cycle performance.

3.4.1 Governing equations

All flames simulated are assumed to be steady state, they do not move upstream or downstream. With the assumption that all properties vary in one direction only, and there is no change with time, the governing equations reduce to their x-direction as all velocities in other directions are zero and all derivatives in other directions are zero. The flame is modeled as a steady state, freely propagating premixed laminar flame in one dimension. From the detailed analysis done in Chapter 7 of [9]:

The continuity equation:

$$\frac{d\dot{m}''}{dx} = \frac{d}{dx}(\rho u) = 0 \tag{3.17}$$

35

The energy equation:

$$\rho u c_p \frac{dT}{dx} + \frac{d}{dx}\left(-k\frac{dT}{dx}\right) + \sum_{i=1}^{N} \rho Y_i \nu_{d_i} c_{p_i} \frac{dT}{dx} = -\sum_{i=1}^{N} \bar{h}^o_{f,i}(T) \cdot \dot{\omega}_i \tag{3.18}$$

The species mass equation:

$$\rho u \frac{dY_i}{dx} + \frac{d}{dx}(\rho Y_i \nu_{d_i}) = M_i \dot{\omega}_i \tag{3.19}$$

The momentum equation: Gravity and viscous terms are neglected, also known as the Euler equation for inviscid flow:

$$u\frac{du}{dx} = -\frac{1}{\rho}\frac{dP}{dx} \tag{3.20}$$

$$u\frac{du}{dx} = \frac{d}{dx}\left(\frac{1}{2}u^2\right) \approx 0 \implies \frac{dP}{dx} = 0 \tag{3.21}$$

where it is assumed that the kinetic energy is constant on a large scale, causing the pressure variation to disappear. This does not mean that velocity is constant, the continuity equation (Eq. 3.17) gives a relation for velocity u. Observe that the product ρu must be constant for its derivative to be zero, indicating that ρ and u are inverse functions of x.

3.4.2 Newton's method for a nonlinear system

A system of nonlinear ordinary differential equations is formed from Eqs. 3.18 and 3.19. Cantera uses a variant of the Newton-Raphson method (more commonly Newton's method). [9] also presents this method, the current section is a summary of Pages 720 - 721. The general method writes:

$$x_{k+1} = x_k - \frac{f(x_k)}{\frac{df}{dx}(x_k)} \tag{3.22}$$

where k is the iteration. Eq. 3.22 is applied to a system of n equations:

$$f_i(x_1, x_2, ..., x_n) = 0 \tag{3.23}$$

where i ranges from 1 to n, the number of equations. A Taylor expansion about $x + \delta$ is used to linearize the system of equations where second-order and higher terms are truncated.

$$f_i(x_1 + \delta_1, x_2 + \delta_2, ..., x_n + \delta_n) = f_i(x_1, x_2, ..., x_n) + \frac{\partial f_i}{\partial x_1}\delta_1 + \frac{\partial f_i}{\partial x_2}\delta_2 + ... + \frac{\partial f_i}{\partial x_n}\delta_n \tag{3.24}$$

The equations are on the form $f_i(x_1, x_2, ..., x_n) = 0$, thus must $f_i(x_1 + \delta_1, x_2 + \delta_2, ..., x_n + \delta_n)$ approach zero at the solution. Only the right hand side of Eq. 3.24 remains and from this a problem on matrix form can be expressed:

$$\left[\frac{\partial f}{\partial x}\right] \cdot [\boldsymbol{\delta}] = -[\boldsymbol{f}] \tag{3.25}$$

where the partial derivative is a matrix known as the *Jacobian*. $[\boldsymbol{\delta}]$ and $[\boldsymbol{f}]$ are column vectors. Eq. 3.25 can be solved with Gauss elimination where $[\boldsymbol{\delta}]$ is the vector to obtain. With $[\boldsymbol{\delta}]$ obtained the next iteration is calculated:

$$[\boldsymbol{x}]_{n+1} = [\boldsymbol{x}]_n + [\boldsymbol{\delta}]_n \tag{3.26}$$

Note that this equation is the result of inserting Eq. 3.25 in Eq. 3.22. This process of iterating continues until convergence is obtained with acceptable error. This numerical method is implemented in, for instance, the internal function *domain.solve(options)*, written by the Cantera developers [26].

[9] mentions that a weakness of this method is the fact that the Jacobian matrix must be calculated for every iteration. The matrix is calculated with a finite difference numerical scheme for all variables, if a detailed kinetic mechanism with many species is used, the computational effort will increase accordingly. This process must be performed for every grid point.

3.4.3 Flame simulation

The scripts handling flame simulations are also based on example scripts written by the Cantera developers. The Python-example *adiabatic_flame* is the base of the script solving the flame structure, this example is chosen as it assumes constant pressure and adiabatic conditions. The solving procedure is unchanged from the example script, while the initial definition of the gas object has been modified to enable automated running of flame simulation with different input parameters (i.e. for-loops). Fig. 3.6 is the core part of the script where the gas object is defined and solver is called.

```python
22    # IdealGasMix object used to compute mixture properties, set to the state of the
23    # upstream fuel-air mixture
24    gas = ct.Solution('chem_CRECK.cti')
25    gas.TPX = Tin, p, reactants
26
27    # Set up flame object
28    f = ct.FreeFlame(gas, width=width)
29    f.set_refine_criteria(ratio=3, slope=0.06, curve=0.12)
30    f.show_solution()
31
32    # Solve with mixture-averaged transport model
33    f.transport_model = 'Mix'
34    f.solve(loglevel=loglevel, auto=True) # Solve with the energy equation enabled
35    f.show_solution()
36    print('mixture-averaged flamespeed = {0:7f} m/s'.format(f.u[0]))
37    f.save('C7_adiabatic_mix.xml', 'mix', 'solution with mixture-averaged transport')
```

Figure 3.6: Screenshot of the script adiabatic_flame, developed by [11].

Line 24 defines the gas object with the kinetic mechanism as input, and Line 25 sets the initial temperature, pressure, and molar fractions. The flame object is created in Line 28, and a mixture-averaged transport model is chosen in Line 33. Finally, the command to solve the problem is called in Line 34. Due to limited experience with programming in Python, the standard objects and commands are chosen, rather than developing own code. The solving procedure follows the nonlinear Newton's method described in the previous section, see the Cantera documentation [26] for details.

Transport model: As seen in Line 33 in Fig. 3.6, Cantera enables the user to chose a diffusive transport model. The model enables computation of the diffusion terms in Eqs. 3.18 and 3.19. Cantera directly computes the diffusive mass fluxes j_i from two possible methods rather than the relation $j_i = \rho Y_i \nu_{d_i}$. The first method uses mixture-averaged diffusion coefficients for each substance while the other method uses multicomponent diffusion coefficients. Thus, there is an option to use a multicomponent transport model or a mixture-averaged transport model.
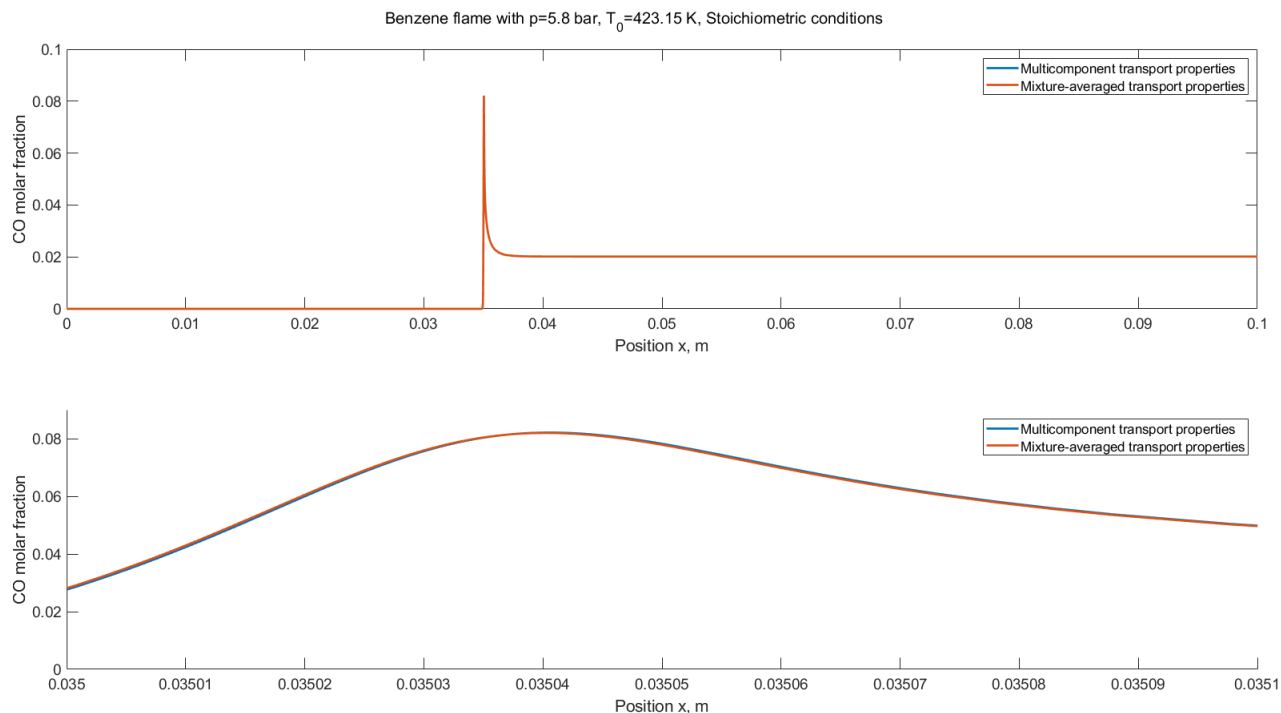

Figure 3.7: Comparison of flame simulation with multicomponent and mixture-averaged properties.

In practice there are only minor differences observed when using the two models. Fig. 3.7 is the result of a premixed laminar flame simulation with benzene as working fluid. The upper plot is how the molar fraction of carbon monoxide evolved throughout the flame length. The lower plot is an expansion of the upper, located at the peak of the upper plot, observe the x-axis. The two graphs generated by the different transport models are close to equal, the multicomponent transport model is slightly shifted to the right. Fig. 3.7 reveals that the shifting length is below 1 micrometer. From this, it is assumed that the choice of transport model has minor influence on the flame structures. The mixture-averaged transport model is chosen, as computation is a little faster with this model, compared to the multicomponent transport model.

Iterative grid refinement: Line 29 in Fig. 3.6 sets the tolerances for the grid points. The flame structure is solved with the initial grid points. If any mass fraction or temperature change too much from one grid point to another, a new point is inserted in between them, and the flame structure is solved once again. The limit for how much a property can change between two points are set by the internal command *set_refine_criteria*. Its input arguments are related to the curves formed by a property. Take the curve which describes mass fraction of O_2 as function of length x. If this curve has a slope or curvature exceeding the input values the tolerance is broken and a new point must be added. See the Cantera documentation [26] for more information.

The grid refinement process is one of the more demanding processes when solving flames. In Cantera, it is iterative, meaning that many attempts may be needed to satisfy the tolerances at all locations. Secondly, the tolerances must be checked for all properties. If a detailed kinetic mechanism is used, this means checking the tolerances for several hundred species. Another issue is that it is not obvious which values to set for the input arguments. The practice used here is simply trying and failing. This sums to a high computational effort. The optimal strategy would be a fine mesh grid prior to refinement to reduce the iterations needed, but this would in turn require far more storage space.

3.5 Results, combustion analysis

Results obtained from the discussed methodology are presented. The main results of interest are the combustion properties at Φ close to unity. Near $\Phi = 1$ the heat released is at its peak, meaning hotter and more concentrated flames. If Φ cannot take this value even as $p_{gas} \rightarrow p_{amb}$ then the Φ-limit introduced in Section 3.2.2 (where the pressure of the gas phase is equal to ambient pressure) is of interest. Values for Φ causing flames with end temperature close to the initial temperature in ignition simulations can be of interest as this can establish self-sustaining flames.

3.5.1 Evolution of Φ

Eqs. 3.11 and 3.13 are plotted with pressure of gas phase on low-pressure side as variable. Fig. 3.8 plots the n-pentane (red) and benzene (blue) cycles in a semi-logarithmic plot. Notice how similar the plot is to Fig. 2.18, it is as if it was mirrored about the horizontal axis, which is due to the inverse dependency $\frac{p_{WF_v}}{p_{gas} - p_{WF_v}}$. This is a consequence of the definitions being close to inverse of each other, compare Eq. 2.20 and Eq. 3.11 for instance.
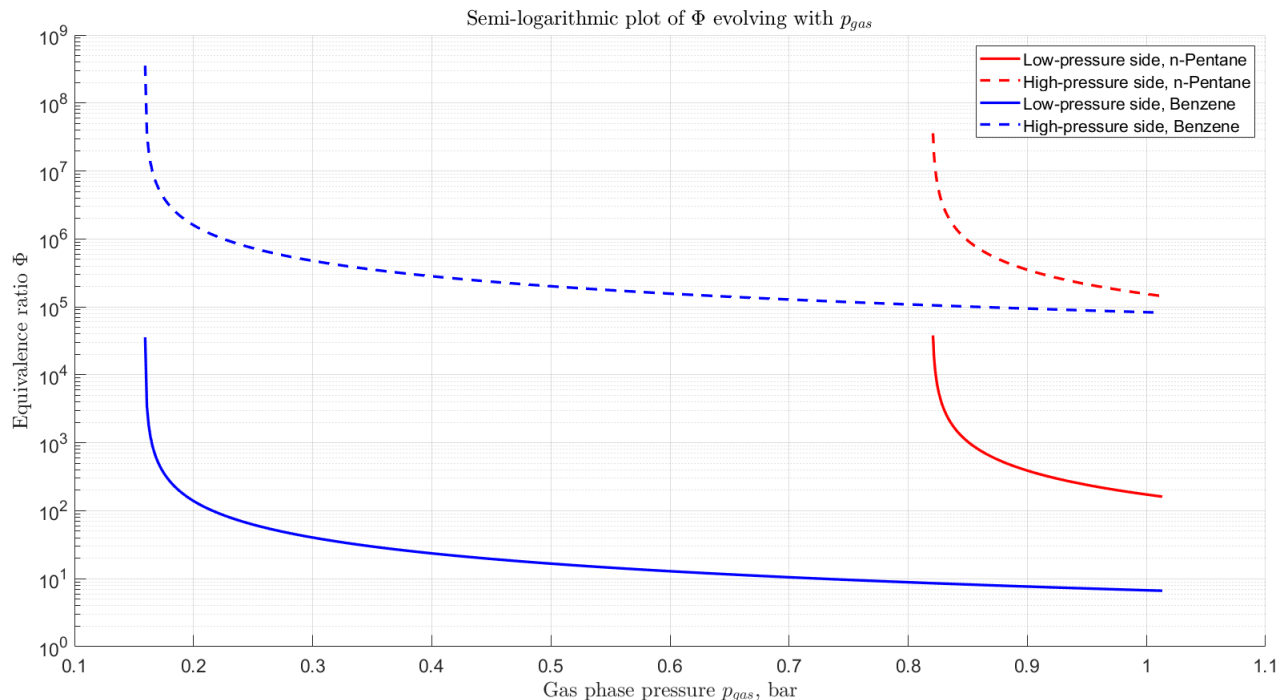

Figure 3.8: Evolution of Φ at State 1 (solid lines) and State 3 (dashed lines) in Fig. 2.1.

Fig. 3.8 reveals that the equivalence ratio Φ is far higher on the high-pressure side, as only the air solved in working fluid is allowed to pass to this side of the cycle. There is a significant difference in Φ on the low-pressure side for the two working fluids, this difference is much less pronounced on the high-pressure side. What seems to be similar for both sides of the cycle is that when using benzene as working fluid the equivalence ratio quickly drops when p_{gas} moves a little from p_{WF_v}, while the case with n-pentane has a more gradual decrease. Unlike what was observed in Fig. 2.18, change in Φ for benzene is still significant as $p_{gas} \rightarrow p_{amb}$.

The limit for equivalence ratio was defined earlier as the value Φ takes when the gas phase pressure is equal to ambient pressure. Φ-limits on the low-pressure side greatly depends on which working fluid is used. Benzene has $\Phi \approx 10^1$, while n-pentane has $\Phi \approx 10^2$ at the limit. Both working fluids has a $\Phi \approx 10^5$ on the high-pressure side at the limit. Thus, there are two trends to observe. The lower the evaporation pressure in an organic Rankine cycle, the lower the magnitude of Φ on low-pressure side, while the magnitude of Φ is close to unchanged on the high-pressure side. This may not hold for fluids where the solubility relations are much different from Eqs. 2.18 and 2.19. There are no cases where Φ is unity, meaning that the Φ-limits are of significant interest.

3.5.2   Results from ignition analysis

The output from ignition simulations are species mass fractions and temperature at all instances, which can plot evolution of all properties with time as the gas volume undergoes ignition. Simulations were done with given Φ and corresponding gas pressure, found from Fig. 3.8. The figure has 200 data points. It is not feasible to run a simulation for all these points, but rather points $[1, 2, 5, 10, 25, 50, 75, 100, 150, 200]$. These are chosen based on their ability to give a discrete yet accurate replication of the curves shown in Fig. 3.8. Figs. 3.9 and 3.10 show that the accuracy is retained to a certain degree. Results from data points $[2, 10, 50, 100, 200]$ (every other) are plotted to avoid cramped plots. Initial temperatures have been set to $T_0 = 500°C$ and $T_0 = 1000°C$.
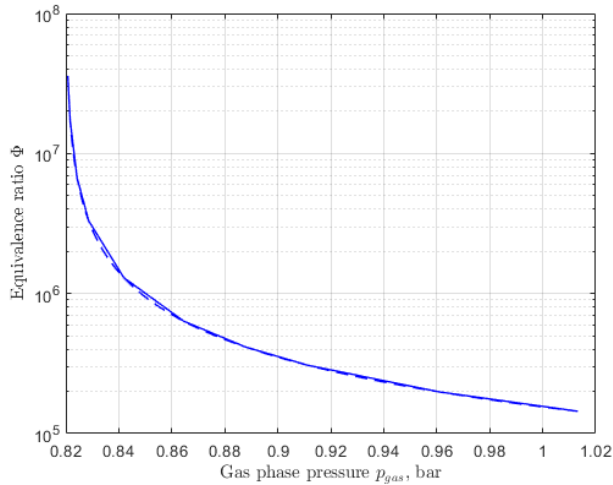

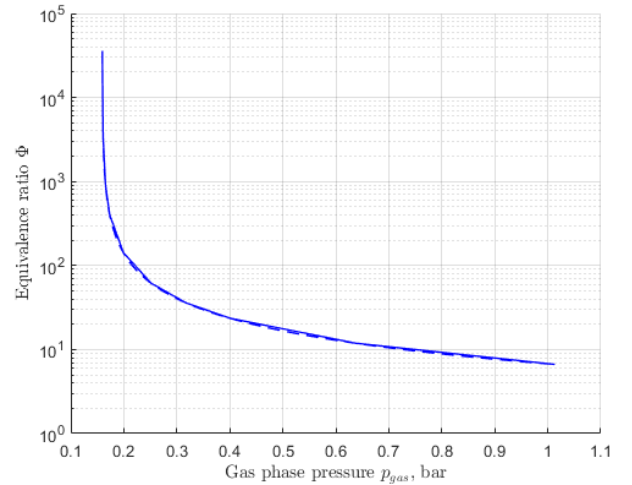Figure 3.9: Evolution of Φ on high-pressure side in n-pentane cycle.

Figure 3.10: Evolution of Φ on low-pressure side in benzene cycle.

Low-pressure side: Figs. 3.11 to 3.14 are temperature plots as function of time from ignition simulation on the low-pressure side. The green curve is the simulation performed at the Φ-limit. Observe that a combustion process is only occurring for certain values of Φ in Fig. 3.12.

The simulations with n-pentane as working fluid seems to have a Φ-limit far above what is combustible at these conditions. The thermal energy provided by the spark is rather spent on anaerobic reactions like decomposition of the working fluid into smaller hydrocarbons, this explains the temperature drop in Fig. 3.11. The temperature graphs in Fig. 3.12 indicate that this also happens in this case after the oxidizer is spent, as there is still much working fluid left. Figs. 3.13 and 3.14 show that little to no reactions occur at $T_0 = 500°$C.

Figure 3.11: Ignition simulation of n-pentane cycle on low-pressure side, $T_0 = 1273$ K.

Figure 3.12: Ignition simulation of benzene cycle on low-pressure side, $T_0 = 1273$ K.

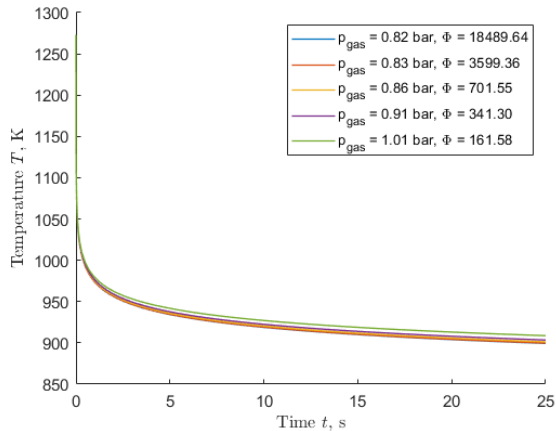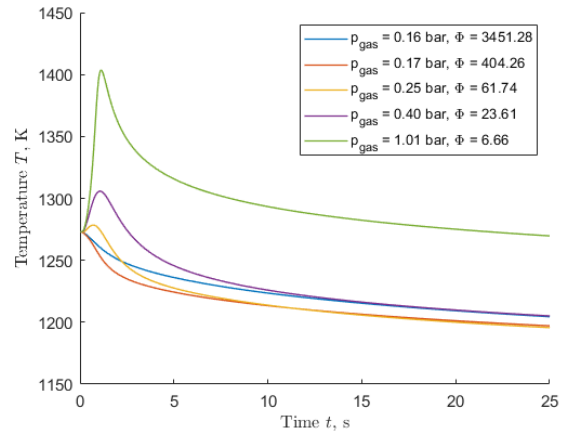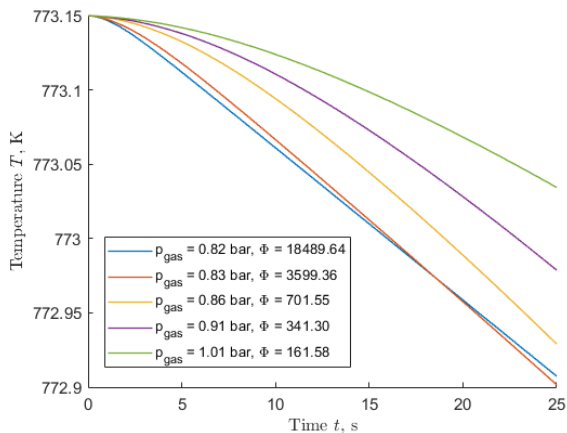Figure 3.13: Ignition simulation of n-pentane cycle on low-pressure side, $T_0 = 773$ K.
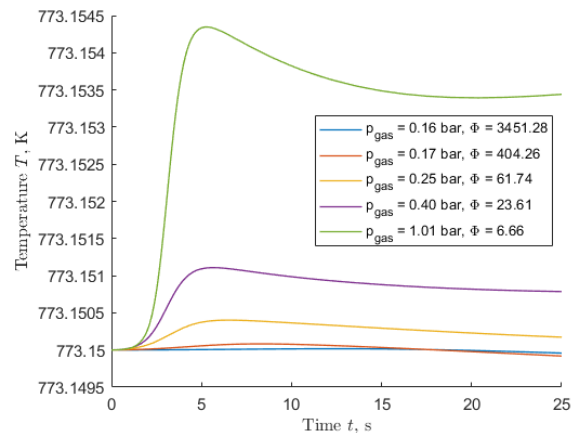

Figure 3.14: Ignition simulation of benzene cycle on low-pressure side, $T_0 = 773$ K.

Ignition is, as stated, observed only in Fig. 3.12 and first occurs when the gas phase pressure has reached 0.25 bar. There are three values of the equivalence ratio that are of interest in Fig. 3.12, $\Phi = [61.74, 23.61, 6.66]$. Additional results from simulations with these three values for Φ are plotted in Fig. 3.15. Solid lines are for $\Phi = 6.66$, dashed lines are for $\Phi = 23.61$, and dotted lines are for $\Phi = 61.74$. The coloring follows the legend in the figure. Notice how peak temperature occurs when the oxygen is almost spent. The temperature then decreases as *acetylene/athyne* (C_2H_2) is formed, and this gas in addition to carbon monoxide, CO, are the main products of the ignition for the three values of Φ. Seeing how the temperatures quickly rise and carbon monoxide is formed it is clear that the mixture that makes up the gas phase on the low-pressure side ignites.
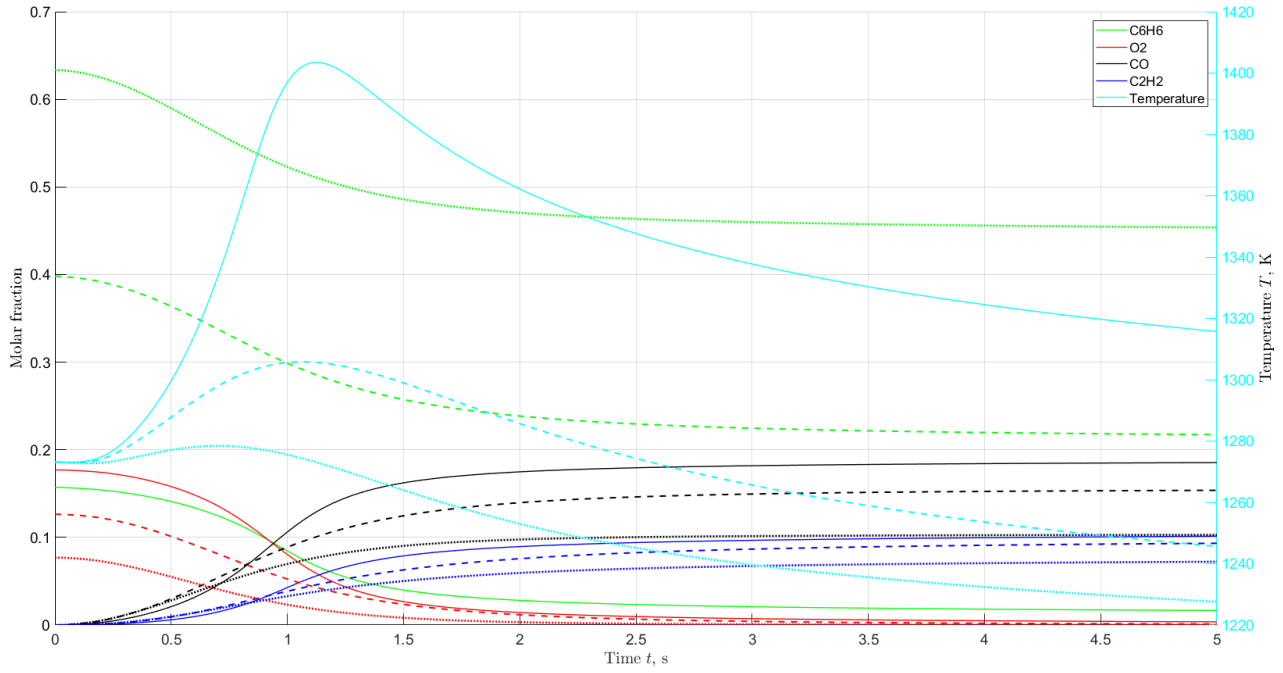
Figure 3.15: Benzene ignition simulation on low-pressure side for $\Phi = 6.66$ (solid), $\Phi = 23.61$ (dashed), and $\Phi = 61.74$ (dotted) with intial temperature $T_0 = 1273$ K.

The cycle using benzene as working fluid is prone to ignition on the low-pressure side if sparks raise T_0 to 1000°C.

High-pressure side: The limits for Φ on the high-pressure side are quite high for both working fluids. Figs. 3.16 and 3.17 shows no signs of ignition. Rather than ignition, chemical reactions not involving oxidizer are taking place. Fig. 3.16 gives a clear indication that endothermic and exothermic reactions are occurring as the temperature drops by 400 K and then jumps back up by 350 K, and this is the case for all the five different values of Φ. Thus, this is not caused by any oxidizer present. The benzene cycle has a far less pronounced effect in Fig. 3.17. Φ and p_{gas} are associated through Eq. 3.13.
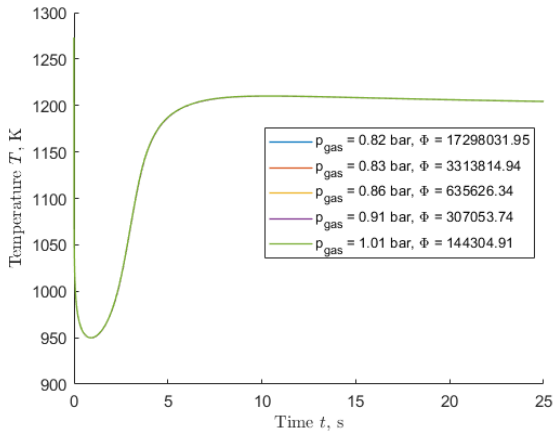

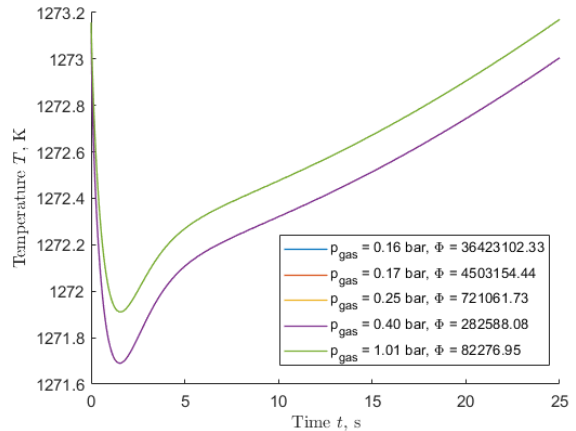Figure 3.16: Ignition simulation of n-pentane cycle on high-pressure side, $T_0 = 1273$ K.

Figure 3.17: Ignition simulation of benzene cycle on high-pressure side, $T_0 = 1273$ K.

A closer look at the n-pentane simulation done at the Φ-limit on the high-pressure side for a n-pentane cycle, the green line in Fig. 3.16, reveals that the n-pentane is broken down into smaller hydrocarbons, see Fig. 3.18. From the figure it is observed that lesser hydrocarbons like butane, propane, and ethene are formed when consuming the working fluid, and these hydrocarbons eventually end up as methane. These reactions are taking up or liberating heat, causing a change in temperature as observed. The time interval of Fig. 3.18 matches that of the temperature change in Fig. 3.16. This decomposition was not found in the simulation done with benzene as working fluid, Fig. 3.17.
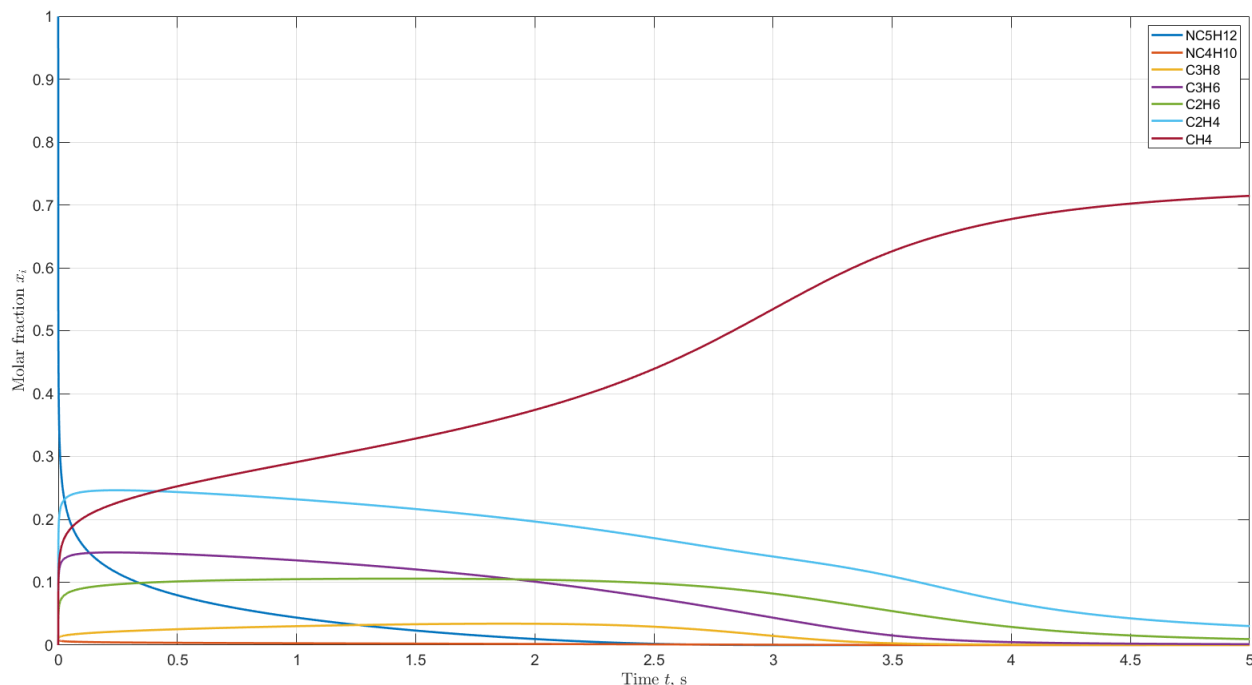

Figure 3.18: Ignition simulation of n-pentane cycle on high-pressure side with $T_0 = 1273$ K, $\Phi = 144304.91$ (limit). Evolution of molar fraction of certain species.

3.5.3 Results from flame structure analysis

Flame structures are solved numerically through the simulations for both the low-pressure and the high-pressure side of the cycle. The input parameters temperature and pressure are set by the non-reactive flow analysis found in Table 2.1, where low-pressure side simulations use State 1, and high-pressure side simulations use State 3. Simulations are performed for 10 logarithmic equally spaced values of $\Phi \in [0.10, 10000.00]$, this range is to be related to the non-reactive flow later in this section. Lastly, a time limit is imposed on the ignition simulations. The flame simulations uses the boundary conditions presented in Section 3.2.1, but flames with flame lengths on the scale of 100 meters must of course be limited.

Low-pressure side: Figs. 3.19 and 3.20 show the flame temperature at all grid points for various values of Φ and at the limits. The horizontal axis reveals flame length, observe how the flames spanning from $x = 10^{-2}$ to $x = 10^0$ have a quick rise in temperature and generally reach higher temperatures than those spanning from $x = 10^1$ to $x = 10^2$.

The latter are far longer and have a more distributed increase in temperature, and are not really flames as the heat release is poor and far from concentrated. In the values of Φ simulated there is a clear threshold between the thin and elongated flame structures. Fig. 3.19, where n-pentane is used, seems to have this threshold somewhere around $59.95 < \Phi < 215.44$. Fig. 3.20, where benzene is used, seems to have this threshold somewhere around $16.68 < \Phi < 59.95$.

Figure 3.19: Flame simulations on the low-pressure side with n-pentane as working fluid.
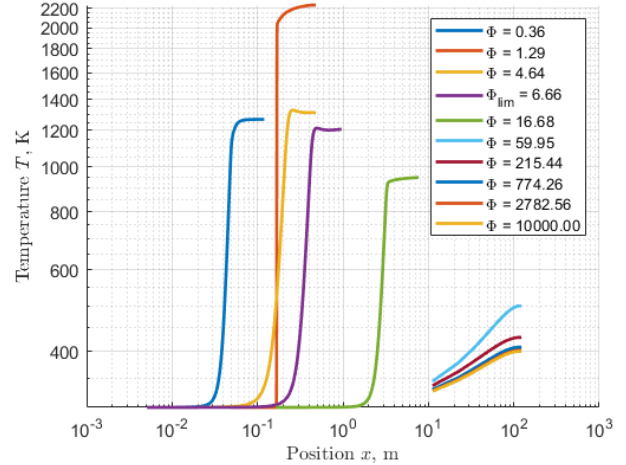
Figure 3.20: Flame simulations on the low-pressure side with benzene as working fluid.

The value for Φ closest to unity when using benzene as working fluid, was found in Fig. 3.8 and is set to $\Phi = 6.66$. The flame structure found at this value of the equivalence ratio is presented in Fig. 3.21. The majority of heat release and substance formation/destruction occurs over 20-30 centimeters and the adiabatic flame temperature is close to 1200 K.
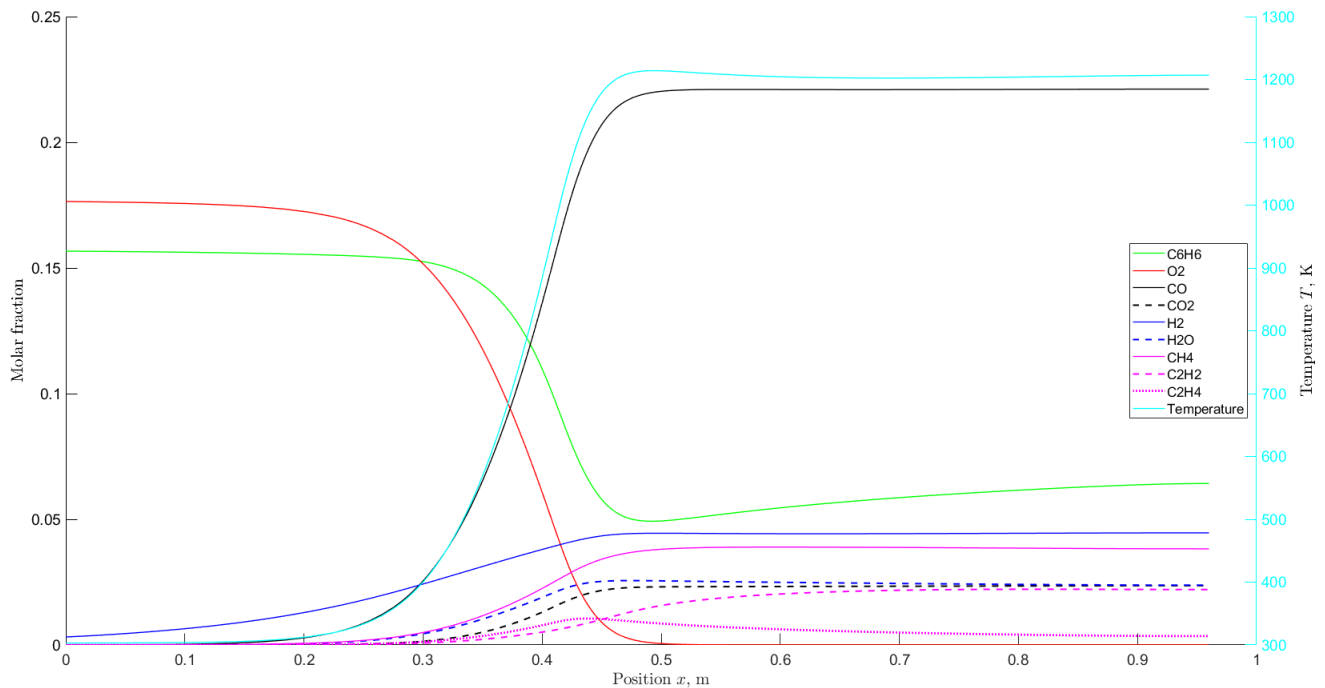
Figure 3.21: Structure of a flame on the low-pressure side of a benzene-cycle with $\Phi = 6.66$.

Fig. 3.21 presents substances of interest involved in the combustion process. Working fluid and oxygen are consumed, and water and carbon monoxide and -dioxide are among the products. Hydrogen gas and methane are also present in the exhaust. Hydrogen and methane are maybe less expected exhaust gases but they are caused by the lack of oxygen which would normally break them down to form water and carbon monoxide. The final observation is that the molar fraction of working fluid increases after $x = 0.5$ meter while the molar fraction of ethene decreases.

Fig. 3.22 presents the flame structure found at the value of Φ closest to unity when using n-pentane as working fluid, with the limit of the equivalence ratio being $\Phi = 161.58$. The figure reveals that not much is happening over a 120 meter long span, and that little to no combustion processes are occurring. The molar fractions of oxygen and working fluid are close to unchanged, no products are formed, and the temperature increases to 390 K. This increase in temperature must come from a change in molar fractions for a set of certain substances, but the substances were unfortunately not identified.
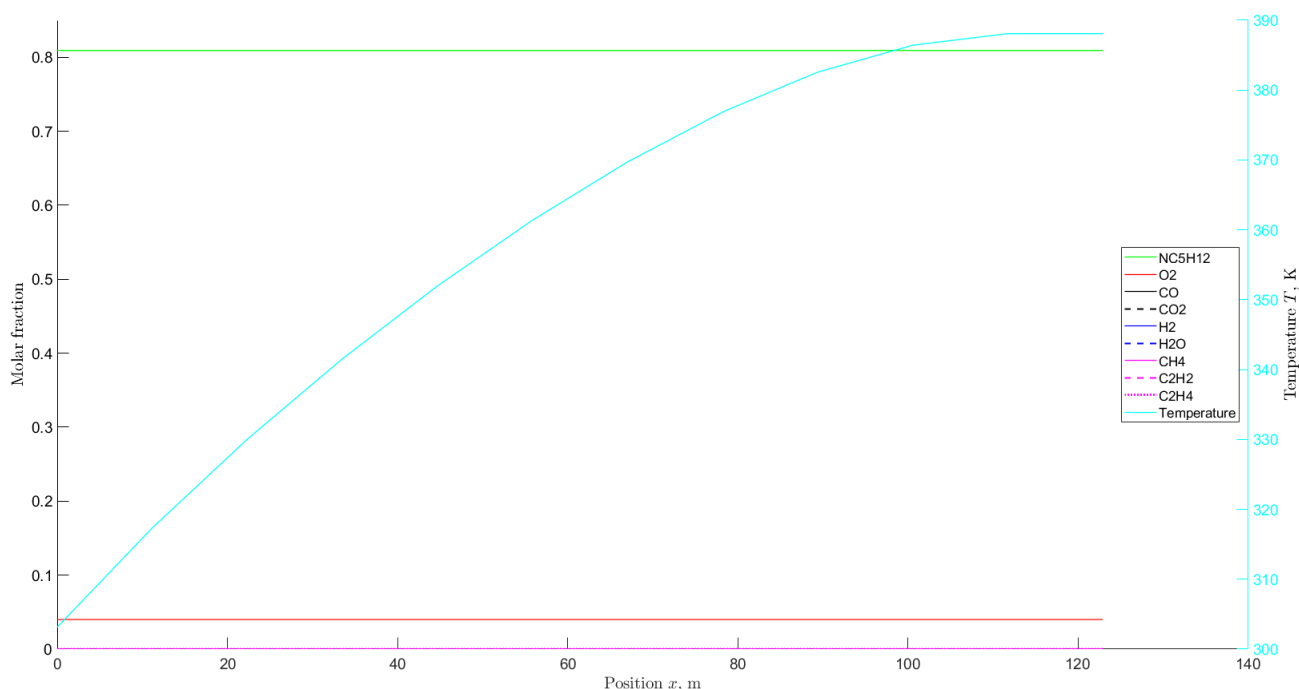
Figure 3.22: Structure of a flame on the low-pressure side of an n-pentane cycle with $\Phi = 161.58$.

From Figs. 3.19 to 3.22 it is evident that flames can appear on the low-pressure side of an organic Rankine cycle using benzene as working fluid. The flame analysed at the limit of the equivalence ratio is indeed self-sustaining as it has adiabatic flame temperatures well above the temperature needed to ignite a gas volume at these conditions, as seen in Fig. 3.15. The cycle using n-pentane is not prone to flames appearing due to its high Φ-limit. Fig. 3.11 reported that no major amount of ignition occurs either.

High-pressure side: The interval $\Phi \in [0.10, 10000.00]$ is far below the limits of Φ set by Fig. 3.8 for the high-pressure side, for both fluids. The limits for the high-pressure side relies on the assumption that only air solved in liquid can pass the pump. If this assumption does not hold it is possible that the Φ-limits can be higher. Thus, simulations are performed for the interval only as high values of Φ have no chance of forming flames due to the lack of oxidizer.
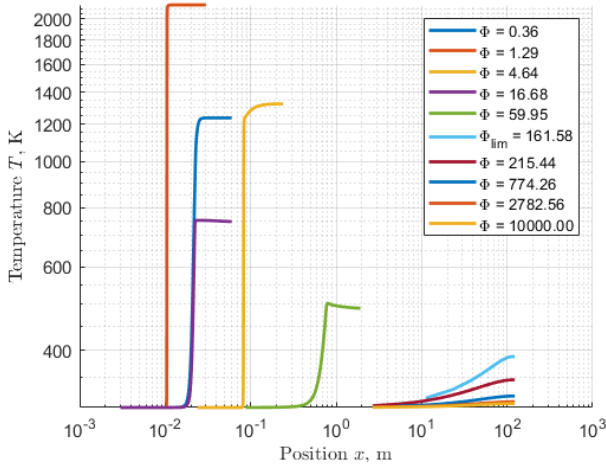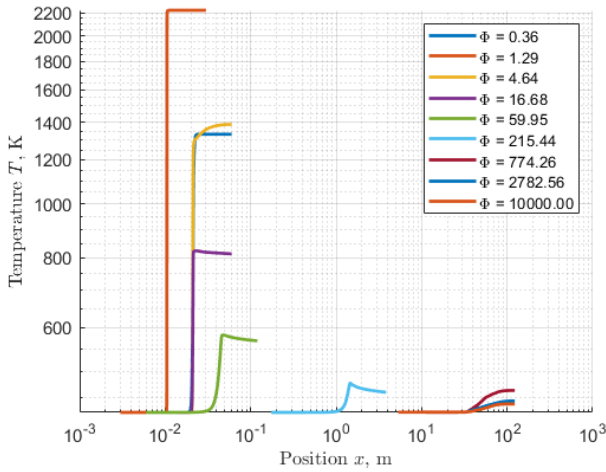
Figure 3.23: Flame simulations on the high-pressure side with n-pentane as working fluid.
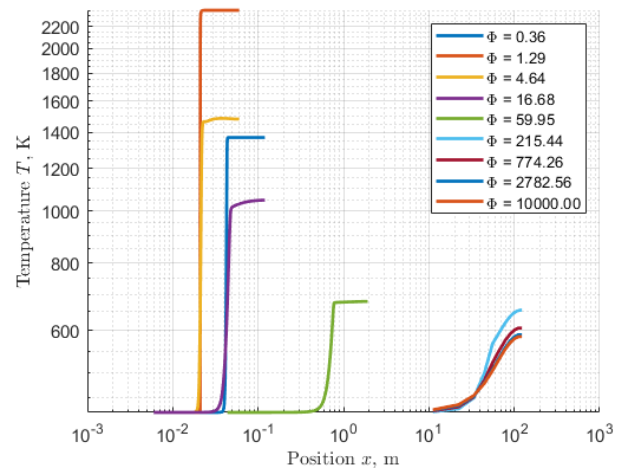
Figure 3.24: Flame simulations on the high-pressure side with benzene as working fluid.

Figs. 3.23 and 3.24 illustrate which values of Φ that allows for flames to appear. A clear threshold is also present here, when $\Phi > 59.95$ the flames are less concentrated and have a minor increase in temperature. The limits found for Φ on the high-pressure side was $\Phi = 144300$ and $\Phi = 82277$ for the n-pentane and the benzene cycle, respectively. The values are far above the threshold and thus can no flame form, meaning that the high-pressure side is neither prone to ignition nor the appearance of self-sustaining flames. This is backed by Fig. 3.25 which shows that no combustion is happening at $\Phi = 10000.00$ for both working fluids.
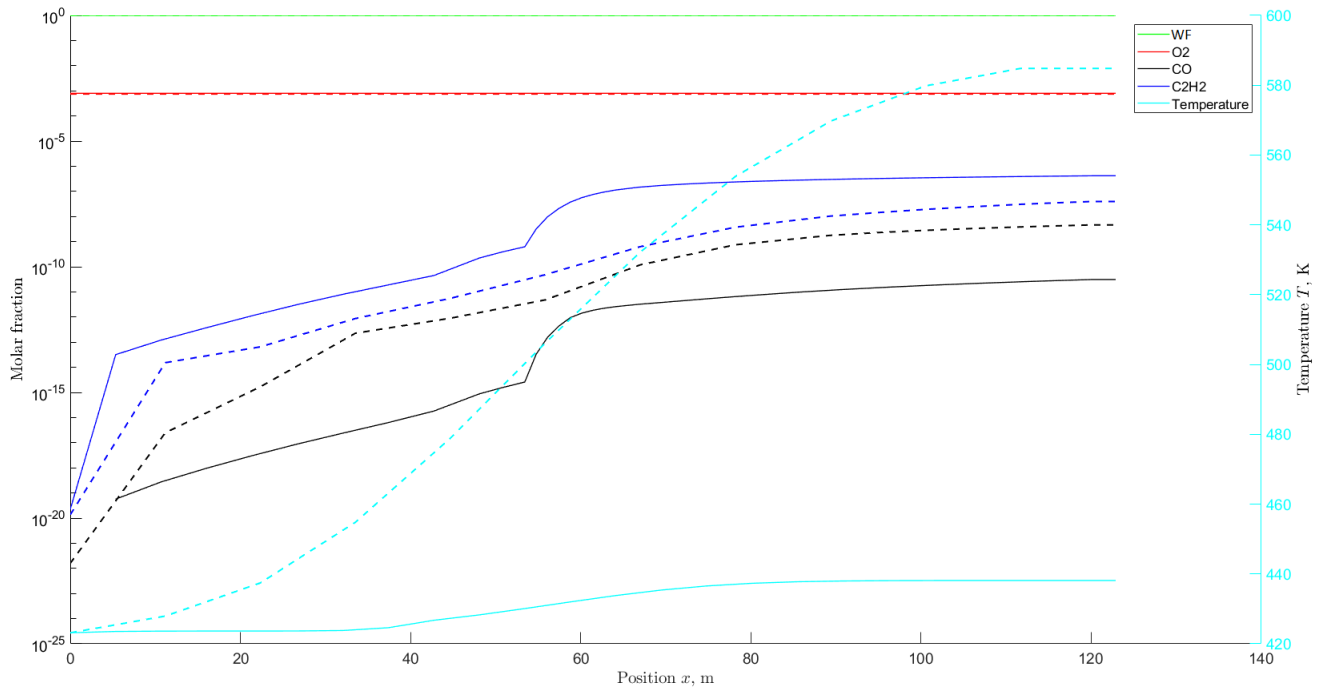
Figure 3.25: Structure of a flame on the high-pressure side of a n-pentane (solid) and a benzene (dashed) cycle, with $\Phi = 10000.00$.

46

DISCUSSION

"What are the consequences of allowing air into an organic Rankine cycles operating with a subatmospheric pressure?"

This question was initially posed as the main objective of this thesis, and was refined into questions for non-reactive and reactive flow. It is to be answered using methodology and results presented in Sections 2 and 3. Various other topics of interest like how the base cycle design influences risks and consequences are also discussed.

4.1   Non-reacting flow

Air was allowed to mix with the working fluid and form a two-phase mixture downstream of the inleak location without reacting with the working fluid. Following what was outlined in the introduction regarding non-reactive flow, the mixture properties and cycle stop were of interest.

4.1.1   Mixture properties

With the introduction of air, there were two species present in the gas phase at the location of inleak and further downstream. The only assumption made regarding breach location and shape was that air must enter such that phase equilibrium is reached for the working fluid at the condenser outlet. The pressure of the gas phase on the low-pressure side was used as a free variable. Fig. 2.18 showed that choice of working fluid has major influence on gas phase composition, n-pentane and benzene took significantly different values.

Relations for flow rate on the high-pressure side used the molar flow rate of air divided by the molar flow rate of working fluid, $\dot{n}_{air}/\dot{n}_{WF_0}$, as input in addition to p_{gas}. Several attempts were made to relate the two through ideal gas law or humidity relation, without success. The ratio of molar flows was only used in the equations for GVF and molar flow rate on high-pressure side, and these relations were only evaluated at the pump inlet. This means that $\dot{n}_{air}/\dot{n}_{WF_0}$ is only a relevant parameter at the pump inlet. $\dot{n}_{air}/\dot{n}_{WF_0}$ could increase at pump inlet if, for instance, phase separation was to occur in the pump, allowing only liquid to pass. This causes an accumulation of gas phase, hence increasing $\dot{n}_{air}$. Lastly, Figs. 2.19 and 2.20 found that choice of working fluid does not greatly influence the molar fraction of air on the high-pressure side, this is a property of the solubility relations used, Eqs. 2.18 and 2.19.

4.1.2 Pump model and cycle stop

A gear pump was investigated based on its applicability for organic Rankine cycles [6][7]. Judging from an experimental study performed on a gear pump, pumping liquids with a viscosity below a certain threshold caused the volumetric flow rate to drop as illustrated in Fig. 2.8. This was caused by backwards flow through clearances between rotating and stationary components inside the pump [7]. The gas phase (air and hydrocarbon vapor) typically have low viscosity and could slip through the clearances found in a gear pump.

It was hypothesized that sufficient amounts air present in the cycle could bring it to halt. From the literature review of multiphase pumping in Section 2.5.2, it became clear that a centrifugal pumps are exposed to phase separation at pump inlet [8], and that this can indeed block the liquid flow to the pump, eventually stopping the cycle. The gas volume fraction (GVF) was used to quantify the amount of gas phase present at pump inlet, at GVF $\approx$ 0.3 the pump lost its performance. This was shown by Figs. 2.10 to 2.12.

If the gas phase is indeed flowing backwards during multiphase pumping with a gear pump, the pump could experience an accumulation of gas at its inlet, blocking the flow. The previous section argued that $\dot{n}_{air}/\dot{n}_{WF_0}$ is only evaluated at pump inlet and that accumulation of would increase the ratio. The developed relation for GVF (Eq. 2.17) allowed for an estimation of the limit values of $\dot{n}_{air}/\dot{n}_{WF_0}$ as function of p_{gas} when using 0.3 as a limit for GVF. An interpretation of this result is that when enough air has accumulated at pump inlet the pump performance drops to nil. It should be noted that GVF = 0.3 comes from an experimental study on a centrifugal pump and cannot necessarily be imposed on a gear pump. If a study is able to find a GVF limit for a gear pump this could be used to determine a limit for $\dot{n}_{air}/\dot{n}_{WF_0}$.

4.2 Reacting flow

4.2.1 Mixture ignition

It was observed that the air and working fluid mixture would only ignite under certain conditions. The first was initial temperature. A comparison between Figs. 3.17 and 3.14 made it obvious that the air and benzene mixture is not heated sufficiently at 500°C, but was able to ignite at 1000°C. Williams' criterion for ignition stated that a heat source must heat the gas to approximately its adiabatic flame temperature, 500°C is clearly insufficient. The ignition criterion is typically used to compute ignition energy, but this is not covered here, a procedure can be found on Pages 295-297 in [9]. A further study could evaluate the ignition energy required at the different values of Φ and investigate how much energy a typical spark can deliver to the gas mixture, determining whether the mixture can ignite or not. This removes the need for arbitrary initial temperatures.

The case with n-pentane was different, as shown in Figs. 3.11 and 3.13, ignition cannot occur for the specified initial temperatures, due to the high equivalence ratio. Raising the initial temperature only brings dissociation of fuel, which is an endothermic process and not ignition. n-Pentane on the high-pressure side was interesting, as a significant drop in temperature was observed in Fig. 3.16, and anaerobic reactions occurred, the working fluid is completely broken down after 2.5 seconds. It is hard to believe that this result is physical, especially as it contradicts what was observed on the low-pressure side in Fig. 3.11, where temperature was strictly decaying as time progressed. The difference between these two simulations is that the pressure is 0.159 at low-pressure and 5.80 bar at high-pressure, with the high-pressure case having significantly higher values for Φ for all simulations.

4.2.2   Flame structures

Simulated flames were only self-sustaining for the cases shown by Fig. 3.20 where Φ was in a range hereby referred to as the self-sustaining range. The range was limited by the limit value of Φ (6.66 for benzene) and an upper threshold. This threshold is somewhere in between $\Phi = 16.68$ and $\Phi = 59.95$ in Fig. 3.20 and was defined in Section 3.5.3 by evaluating flame length and heat release. The ignition plot in Fig. 3.12 showed that ignition can occur for $\Phi = 23.61$ and $\Phi = 61.74$, this last value is outside the recently mentioned threshold, however.

This means that even if ignition occurs the flames are not necessarily self-sustaining. $\Phi = 23.61$ could potentially be within the self-sustaining range as it is not too far from $\Phi = 16.68$, but this data is unfortunately not available. Using Eq. 3.11, $\Phi = [6.66, 16.68, 23.61, 59.95]$ is roughly translated to $p_{gas} = [1.01, 0.50, 0.40, 0.25]$ bar, this shows that flames can be self-sustaining already at $p_{gas} = 0.50$ bar and possibly even lower at $p_{gas} = 0.40$ bar. A further examination of the self-sustaining range could be performed to find a good threshold value, but it is theorized that there is no hard limit for when a flame is self-sustaining or not.

For the organic Rankine cycle using n-pentane as working fluid the results are far less interesting, the equivalence ratio cannot possibly take values below $\Phi = 161.58$ with the states in Table 2.1, and at this value for Φ no combustion is occurring. A simulation performed at that value for Φ on the low-pressure side was shown in Fig. 3.22 and it has rather unrealistic properties. The temperature is increasing with length while no reactants are consumed. A similar observation is done in Fig. 3.25 where both working fluids are simulated. The temperature rises in both cases while the reactants are unchanged. There is an increase in products on the low orders of magnitude but no oxygen is consumed.

4.2.3   Irregularities in combustion simulations

There is an overall trend in flame simulations where Φ takes high values, observed for $\Phi = 161.58$ in Fig. 3.22 and $\Phi = 10000.00$ in Fig. 3.25; the temperature is increasing while no oxidizer is spent. After a through search of possible human errors when plotting without any results it is clear that the plotting is indeed correct and that the data generated from the simulation is strange. Moreover, the iterative grid refinement described in Section 3.4.3 generated less than 20 grid points for a 120 meter long flame, which is far fewer than simulations performed at lower values of Φ. From this it is theorized that grid refinement options and related tolerances are incorrect.

The simulations of ignition processes did not have this issue and generated 200+ grid points and did not show any irregular behaviour, with one exception. A comparison between Figs. 3.11 and 3.16 shows that the low-pressure ignition of n-pentane starting at 1000°C only consumes the thermal energy. However, the high-pressure ignition with equal initial temperature has a gain in temperature after a few seconds. Both cases start with an endothermic process while only the high-pressure simulation has an exothermic process after that. Fig. 3.18 is an attempt at further understanding of these processes, and shows how intermediate species form and are consumed to create methane. This was not observed for the low-pressure case. These processes forming methane are in general not familiar to the author, a possible explanation may be pressure dependence. In any regard, no combustion process is occurring in either case, other processes are beyond the scope of this study.

4.2.4 Soot formation

From the results it has been observed that incomplete combustion dominates the possible combustion processes in an organic Rankine cycle using benzene as working fluid. Though soot is more common in diffusion flames there is a possibility of it forming in premixed flames, a study by Pejpichestakul *et al.* [27] examined this in detail. When selecting a kinetic mechanism in Section 3.2.3 it was argued that mechanisms involving soot formation is left out due to limited time and computational resources. A kinetic mechanism taking soot into consideration is available from [12], but is now consisting of 500+ species and 20000+ reactions.

4.3 Influence of base cycle

It is evident that the base cycle has much influence on the results presented in Sections 2.7 and 3.5. Table 2.1 has three parameters, which were set initially; what working fluid to use and the temperature at States 1 and 3. If the base cycle was redesigned, these would be possible to change, as they did not change during the inleak process. The main output values of interest are molar fractions of air on both pressure sides, equivalence ratio and its limits, and combustion properties presented in Sections 3.5.2 and 3.5.3. These all depend on the base cycle in one way or another.

4.3.1 Condenser outlet temperature

The condenser outlet temperature (State 1 in Fig. 2.1) is in reality set by the ambient temperature and the heat exchanger used as condenser, but for convenience it was set arbitrarily to 30°C. This temperature determines the pressure on the low-pressure side along with the choice of working fluid, as the pressure was set to be the saturation pressure of the fluid at that temperature. It is known that the saturation pressure in general[1] decreases as the temperature takes a lower value. For the two fluid examined in this study, n-pentane and benzene, it is known that they both experience a reduction in saturation pressure if the saturation temperature is decreased from 30°C to 10°C, as an example.

Recall that the pressure of the working fluid in vapor phase, p_{WF_v}, was found to be approximately the saturation pressure at 30°C for both working fluids. From this observation there is reason to believe that a decrease in condenser outlet temperature brings a lower value of p_{WF_v} and consequently allow more air into the cycle as described by Eq. 2.22. According to Eq. 3.11, this allows for values of Φ closer to unity, which brings more heat releasing combustion processes as seen for flames in Figs. 3.19 and 3.20. Conversely, an increase in condenser outlet temperature brings a higher value of p_{WF_v} and constrain the air pressure even further, bringing the values of Φ up, and heat release in the combustion processes down. Lastly, note that the condenser outlet temperature would, according to the model used in this study, only change if design or operation changes were made prior to air inleak. It is assumed to be unaffected by air leaking in. Whether this assumption holds or not is hard to say, if a breach occurred downstream of the condenser it could very well be possible. With a breach upstream of the condenser it may not hold as the heat transfer in the heat exchanger is influenced by the two-phase flow. This is discussed in detail in Section 4.4.2.

---

[1]There are of course exceptions, and the temperature should not take values far from typical ambient temperatures where one would operate an organic Rankine cycle.

4.3.2 Evaporator outlet temperature

The evaporator outlet temperature (State 3 in Fig. 2.1) was in reality set by the temperature of the heat sources supplying the organic Rankine cycle with thermal energy and the heat exchanger used as evaporator. However, similar to the condenser outlet, temperature was set arbitrarily to 150°C, which could represent a low-temperature heat source. With the assumption that working fluid exits the evaporator as saturated vapor and no pressure loss, the pressure on the high-pressure side is set when the working fluid is known. Following the discussion in the previous paragraph, it is known that the saturation pressure increases with increasing temperature, thus will the pressure on the high-pressure side increase with increasing evaporator outlet temperature.

However, this pressure does not have as much influence on mixture composition and combustion as the pressure on the low-pressure side. The numerical value is not used in any computations related to molar fractions, but can be of importance in ignition and flame simulations. Page 280 in [9] states that experimental measures in general reveals that flame speed has an inverse variation with pressure, and points to an experimental study conducted by Andrews & Bradley [28].

4.3.3 Working fluid

The working fluid is by far the most important variable. The results showed major differences in the combustion properties of a cycle using n-pentane compared to a cycle using benzene. Figs. 3.19 and 3.20 showed that for the cases $\Phi \in [0.36, 1.29, 6.46, 16.68]$, the flames where benzene was burning attained a higher temperature. The same figures found a threshold for Φ where flames were not forming. This threshold was closer to unity for benzene than n-pentane. Figs. 3.11 and 3.12 showed that the cycle using n-pentane was unable to ignite at all possible values of $\Phi \in [161.58, \infty\rangle$, while the cycle using benzene ignited for $\Phi \in [6.66, 23.61, 61.74]$. These intervals are directly related to the vapor pressure of the working fluid at 30°C.

The pump model developed in this study stated that air could only be transported through the pump if solved in the liquid flow of working fluid. Eq. 3.13 showed that the solubility of air in working fluid determines the values of Φ on the high-pressure side, and the solubility was determined by the empirical Eqs. 2.18 and 2.19. Obviously, the solubility depends on the working fluid, although it was observed in Fig. 2.18 that the molar fraction of air was of the same order of magnitude for both working fluids at the pressure limit $p_{gas} \to p_{amb}$. No calculations have been performed where the solubility x_1 was found to be very different. Curve 9 in Fig. 2.15 is the solubility of nitrogen gas in n-Hexane, compared to Curve 5, the solubility in n-hexane is one order of magnitude higher.
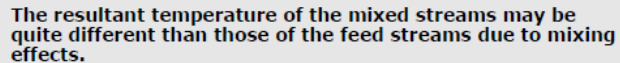
Lastly, choosing a working fluid sets the stoichiometric ratio R_{st}, which again has direct influence on the equivalence ratio. There is a possibility that a working fluid with a set stoichiometric ratio can reach $\Phi_{LP} = 1$ at $p_{gas} \to p_{amb}$, or even before that, given sufficiently low p_{WF_v}.

4.4 Model reliability and validation

All models developed in this thesis must in one way or another be validated by experimental data. This thesis contributed minor amounts to the methodology presented for reacting flow/Section 3, it has been developed and validated over the past decades. The assumptions, relations and models presented in Sections 2.3 to 2.6 must be validated however, as they have been presented in this thesis for the first time and are without experimental data to back them.

4.4.1 Hysys inleak model reliability

Hysys simulations reported a decrease in temperature when mixing air and working fluid as shown in Figs. 2.16 and 2.17. The cycle using benzene as working fluid was able to reach below 0°C, far below the initial temperature. This is intuitively completely wrong. Section 2.7.1 questioned the realism of these results and argued that the user has insight in which equations are used in a commercially available software like Hysys. The mixing operation drawn in Fig. 2.4 was the one causing the change in temperature, when looking the component up at Page 7-16 in [5] no equations are listed. Fig. 4.1 is a screenshot from the page stating that mixing effects can bring non-isothermal mixing.

The resultant temperature of the mixed streams may be quite different than those of the feed streams due to mixing effects.

Figure 4.1: Screenshot of Page 7-16 in [5].

If this is the case then the Hysys inleak model developed in Section 2.3.2 must be verified by other means, as it reported results that are hard to believe. This is why Section 2.3.2 stated that results from a model independent of the inleak model developed in Hysys must be compared to results from the Hysys inleak model. Unfortunately, the two models yield results too different for any meaningful comparison. There was no point in comparing the pump model from Section 2.5 to the pumping operation in Hysys, to use one example. The one found in Hysys originated from thermodynamic analysis while the pump model developed in Section 2.5 is empirical and based on observations from experiments on other pumps. Thus, results from the Hysys inleak model are disregarded as they do not contribute to any of the main objectives.

4.4.2 Validity of assumptions in numerical inleak model

The main outcome of the numerical inleak model was presented in Section 2.6. The problem with many of the developed models is that they build upon assumptions regarding properties of two-phase flow that are hard to validate, some are even subject to modern research. Especially two-phase flow through components like heat exchangers and pumps is hard to model without having data for the exact components.

Phase transition of air: Air was assumed to be purely gas phase when computing the pressure of the working fluid in vapor phase, p_{WF_v}. Later, the air was assumed to solve in the stream of liquid working fluid, contradicting the first assumption. However, solubilities were found to be minor at given conditions and it was therefore theorized that air solving in liquid would not significantly affect partial pressure of air in the gas phase. Of course, a major increase in air density from gas to liquid could mean that much air is compressed into the liquid, which densities air takes when solved in working fluid must also be investigated. The best course of action would be solving phase equilibrium with both fluids, as presented on Page 787 in [3].

Solubility of air: It was assumed that the solubility of nitrogen gas in various hydrocarbons could be extended to be valid for air, not just nitrogen. This assumption must be backed by research on solubility of either air or oxygen gas in the same hydrocarbons, to check if the numerical values can be extended to air and is not limited to just nitrogen. If not, solubility must be evaluated for air as a mixture or oxygen and nitrogen as individual species.

Heat transfer in evaporator: An assumption that has not been addressed yet is that the mixture of air and working fluid is in gas phase when exiting the evaporator. The heat transfer coefficient of a heat exchanger depends on numerous variables, thermophysical properties of the fluid to be heated are one of them. Air is in general associated with low heat transfer coefficients which could cause the stream exiting the evaporator to remain two-phase. This has not been investigated even though it is of great relevance. To perform this investigation knowledge of heat exchangers employed in organic Rankine cycles must be obtained and then analyzed when exposed to two-phase flow. Two-phase flow in heat exchangers are subject to modern research, much like pumps, and may turn out to be quite an obstacle.

Validity of pump model: The pump model dictates how much air is allowed to pass to the high-pressure side and when the cycle stops, and is a critical part of this study. The suggested model assumes no drop in pressure on the high-pressure side and a reduced flow rate, it was developed based on an experimental study of a gear pump where low-viscous fluids were used [7] and an experimental study on pumping an air-water mixture with a centrifugal pump [8]. Thus, the pump model should have some accuracy. However, assuming that only liquid is able to pass the pump was made to enable computation, this must either be confirmed or corrected by experimental results quantifying how much gas phase a gear pump can bring to the high-pressure side.

4.5 Safe working fluids

From the discussion in Sections 4.2 and 4.3 it is clear that using benzene as working fluid carries severe consequences, if air was to leak in and combustion to occur. Conversely, n-pentane showed little to no consequences if air was to leak in, as far less air can mix with the working fluid inside the pipes. At the given outlet temperatures for condenser and evaporator, n-pentane can be regarded as safe to use, while benzene is unsafe. It was clear from the combustion results that Φ determines whether combustion processes occur or not.

If a general procedure on classifying working fluids as safe for subatmospheric organic Rankine cycles or not was to be formulated, it would first of all require the possible range of Φ on the low-pressure side to be computed (Eq. 3.11). The range is dictated by two fluid-specific properties; the stoichiometric ratio, R_{st}, and the equilibrium pressure of the vapor phase, p_{WF_v}. The latter was approximated to be the saturation pressure at the specified temperature. R_{st} is constant, p_{WF_v} varies with temperature. An operating range for the condenser inlet temperature must be specified to find all possible values for p_{WF_v}. It was observed in the figures showing flame temperature varying with Φ, Fig 3.19 for instance, that Φ closer to unity brings more intensive combustion. Thus, the main value of Φ of interest is the closest to unity. However, $\Phi \gg 1$ is not sufficient information to classify an organic fluid as safe. Combustion processes must be simulated at the value of Φ, and the resulting properties analyzed.

The investigations conducted here can state that n-pentane is safe at given temperatures based on simulations, but not necessarily for other values of the condenser outlet temperature. If the condenser outlet temperature was set to 5°C, down from 30°C, the value of Φ closest to unity would be 16.48, down from 161.58. According to Fig. 3.19, self-sustaining flames can now be present on the low-pressure side of the cycle. Combustion on the high-pressure side must also be evaluated, but from the discussion on the pumping operation in Section 4.1.2, there will be more air present on the low-pressure side.

4.6 Breach geometry and transient inleak

Breach geometry: An aspect that has been left out of this thesis the transient process where a subatmospheric organic Rankine cycle is filled with air. Due to the randomness associated with geometry of breaches the transient inleak is hard to evaluate, unless a weak spot was designed into the cycle causing the breach geometry to be known in the event that a breach occurs. A large breach in the piping will cause working fluid to spill out of the cycle, causing a completely different situation than that of air present inside the cycle. In that case, combustible gasses would spill/leak out to the environment. Using an operating pressure on the high-pressure side, sufficiently high to exceed pressure rating of piping and other components, can cause working fluid to leak out. These situations are more similar than when air is leaking in. Thus, large breaches were not relevant in this case.

The instantaneous case: Time scales at which air fills the cycle has not been estimated. However, it is possible to investigate the extreme case where the gas phase pressure instantaneously reaches ambient pressure, as if air entered with a large volumetric flow rate. The average time spent to generate a spark (could be the frequency of a pump or turbine) will be longer than instantaneous. In that case, is combustion only relevant at Φ evaluated at $p_{gas} = p_{amb}$, since no ignition can occur before a spark is generated. Furthermore, if a working fluid whose properties yields $\Phi \ll 1$ at $p_{gas} = p_{amb}$ was used in the cycle, the consequences of combustion could be diminished due to the fact that heat release from combustion at $\Phi \ll 1$ is rather minor (Chapter 8 in [9]). No such fluids were simulated, however. In addition, time spent to bring p_{gas} to p_{amb} depends greatly on piping length.

Material integrity: Fig. 3.21 showed that flames in a cycle using benzene as working fluid could reach up to 1200 K when the low-pressure side was filled with air ($p_{gas} = p_{amb}$). The integrity of many metals, sealants, gaskets, couplings, and valves are compromised at such high temperatures. For instance, the heat exchanger used as condenser is probably not designed to handle such temperatures. If the combustion is releasing sufficient amounts of thermal energy to destroy seals in the exchanger, the combustion is no longer bound to be inside the cycle. In other words, flames can propagate on the outside. More oxidizer is present outside the cycle, but the flames would in that case progress from premixed to diffusion flames.

In the case where the cycle is not punctured by the heat release from combustion, another issue will present itself. It is well-known that increasing temperature brings increased pressure for many gases, as the gas wants to expand but is limited by the volume. All simulations related to combustion assumed constant pressure, but in a confined space the pressure will rise. A very sudden rise could cause explosions. An estimate of the pressure increase for the benzene ignition depicted in Fig. 3.15 is done using Eq. 4.1, which is derived from the ideal gas law. State 1 is before ignition and State 2 is after ignition:

$$p = \sum_{i=1}^{N} p_i = \sum_{i=1}^{N} \frac{n_i R T}{V} \implies \frac{p_2}{p_1} = \frac{T_2}{T_1} \cdot \frac{n_2}{n_1} = \frac{T_2}{T_1} \cdot \frac{M_1}{M_2} \tag{4.1}$$

$$m_1 = m_2 \implies n_1 M_1 = n_2 M_2 \implies \frac{n_2}{n_1} = \frac{M_1}{M_2} \tag{4.2}$$

where a total mass conservation was used to determine the ratio between moles. In Fig. 3.15 the premixed gas is 30°C prior to ignition, and for $\Phi = 6.66$ the temperature ends at ≈ 1320 K.

With $T_2/T_1 \approx 4.6$ and $M_1/M_2 \approx 1.4$, it is found that p_2/p_1 is at least greater than 7.4. If local ignition caused the entire volume on the low-pressure side to ignite, the gas phase pressure could increase to 7.4 atm. This is not an entirely precise calculation, as the computation used to obtain the temperature T_2 assumed constant pressure. It should serve as an order of magnitude, at least. Observe that the pressure has increased beyond the pressure on the high-pressure side.

4.7 Future outlook

Different base conditions: By testing two different working fluids with only one set of temperature conditions it was found that choice of working fluid had major influence. The discussion in Section 4.3 argued that temperature conditions are also of importance. A further study should evaluate evolution of Φ for several different working fluids and temperature conditions, just like what was done in Fig. 3.8. Ignition and flame simulations should be performed at the appropriate conditions (temperature, pressure, equivalence ratio). It would be of interest to see a base condition where the limit of Φ is unity or below.

Pump model validation: From the discussion it is clear that many of the results on the high-pressure side are uncertain, as a series of non-validated assumptions are underlying the models used to obtain them. The most crucial part to validate is the pump model, as this determines all property on the high-pressure side. Experimental data on pumps appropriate for organic Rankine cycles are needed to evaluate two-phase flow in pumps appropriate for organic Rankine cycles.

Further simulation of combustion: Further studies using Cantera should evaluate risk of explosion, ignition energy, quenching, and employ a kinetic mechanism that includes soot formation. The risk of explosion is caused by a rise in pressure, and thus must ignition simulations with varying pressure be performed. These simulations assumed constant gas density, see examples at [26]. Calculating ignition energy is of interest as it would help understanding how much thermal energy sparks must bring the gas volume. With that being known, one could state that cases where ignition energy is on very large scales does not carry risk of ignition. Lastly, an analysis of quenching related to narrow diameters in organic Rankine cycles should also be performed, comparing quenching distance[2] of various working fluids and equivalence ratios to typical diameters in organic Rankine cycles.

Justify subatmospheric pressures: As stated initially in Section 1.2, there are few studies where subatmospheric pressure values are used in organic Rankine cycles. This thesis has not discussed the possible advantages with subatmospheric pressure, other than a possible increased efficiency, without showing any numbers. A future study should investigate the gain from of using subatmospheric pressures, and which organic working fluids are feasible to use regarding increased thermal efficiency. Such a study would contribute in several ways. First of all, it can exclude organic fluids or temperature ranges from further combustion analysis, as some fluids may be polluting, or hard to come by. Secondly, a possibility of increased cycle efficiency would serve as a motivating factor for further studies on air in organic Rankine cycles.

---

[2]Not covered here, see Pages 287-290 in [9].

<div align="right">CONCLUSIONS</div>

5.1 Safety aspects of organic Rankine cycles

Re-addressing the question posed at the start of the discussion, it is clear that allowing air into a subatmospheric organic Rankine cycle brings a multi-component gas phase on the low-pressure side, and gas accumulation at the pump inlet, bringing the cycle to halt. The developed pump model allows only liquid flow to pass to the high-pressure side. Gas flow has too low viscosity, and slips through the clearances in the pump. Only air solved in liquid working fluid can pass to the high-pressure side. No more air can enter the cycle when the gas phase pressure on the low-pressure side has reached ambient pressure. This sets an upper limit for the molar fraction of air, and consequently the equivalence ratio. The upper limit for the molar fraction of air in gas phase is several orders of magnitude higher on the low-pressure side compared to the high-pressure side. The upper limit for the molar fraction of air on the low-pressure side is one order of magnitude higher for benzene than n-pentane.

Ignition and flame simulations reveal that combustion processes can occur on the low-pressure side, when using benzene as working fluid and operating with conditions equal to those in Table 2.1. At the conditions closest to stoichiometric, the resulting flames are self-sustaining and can reach 1000°C, causing major damage to equipment and expanding gases rapidly, which carries a risk of explosion. Under certain conditions the gas phase can ignite, but the resulting flames will quickly die out due to lack of oxidizer. Combustion simulations of a cycle using n-pentane as working fluid and temperatures listed in Table 2.1 show no signs of combustion processes on the low-pressure side at the given conditions. This is a consequence of the high saturation pressure of n-pentane at 30°C, since this pressure along with the ambient pressure limits the maximum amount of air present on the low-pressure side. Combustion simulations on the high-pressure side make it clear that the possible values Φ can take on this side is far higher than what is combustible, the high limit for Φ is a consequence of the developed pump model. However, all processes on the high-pressure side are inconclusive, as the pump model is not validated.

Based on simulation results, benzene is classified as an unsafe working fluid, as it is prone to ignition and can for self-sustaining flames. n-Pentane is classified as a safe working fluid, as it is not prone to combustion, but **only** under the conditions specified in Table 2.1. n-Pentane may not be classified as a safe working fluid under other conditions, unless new investigations are conducted with other conditions. It is evident that these conditions have a major influence on combustion intensity. A general observation is that lower temperatures bring more intensive combustion as more air can enter.

A procedure to classify organic fluids as safe or unsafe as working fluid is outlined. A Φ progressing towards unity brings more intensive combustion processes. A strategy is to define a complete interval for Φ, these intervals can be on the form $\Phi \in [\Phi_{lim}, \infty\rangle$. The value of Φ_{lim} is defined as the equivalence ratio when no more air can enter the cycle. In other words, when gas phase pressure is equal to ambient pressure. The limit of Φ on the low-pressure side strongly depends on the condenser outlet temperature. Φ must be evaluated for a range of operating temperatures, to ensure that a change in cycle operation will not bring a safe working fluid to its unsafe regime. The value of Φ when under the conditions in Table 2.1 is 6.66 for benzene, 161.58 for n-pentane. Unsafe regimes for working fluids are typically $\Phi \leq 10^2$, safe regimes are typically $\Phi \geq 10^2$. Simulation of combustion processes are necessary to ensure that an organic working fluid is in its safe regime.

A series of digital tools are employed in this thesis. The process simulator Hysys is used to simulate non-reacting mixing and flow. The results from these simulations are unfortunately not of use, due to a strong non-isothermal effect that occurs when mixing liquid working fluid and air. Cycle thermal efficiency is computed, but is not of any interest. Cantera is an effective tool for simulating combustion processes. However, with large values for Φ the flame simulations are not accurate, and takes up a lot of computational resources. Integration with kinetic mechanisms is easy, but very complex mechanisms are unfit for flame simulations. Integration between Matlab and the REFPROP makes using thermodynamic data in Matlab scripts very quick and reliable. Compatible with the parallel processing toolbox in Matlab.

Further research on subatmospheric organic Rankine cycles is outlined. Different topics are suggested as relevant progress, among them is the need for investigating if subatmospheric cycles are indeed feasible regarding increased efficiency. Other topics are non-constant pressure ignition, investigation of the effect of various base cycle properties regarding combustion processes, and validation of the inleak model developed in this thesis.

References

[1]   Michael Papapetrou, George Kosmadakis, Andrea Cipollina, Umberto La Commare, and Giorgio Micale. "Industrial waste heat: Estimation of the technically available resource in the EU per industrial sector, temperature level and country". In: *Applied Thermal Engineering* 138 (2018), pp. 207 –216.

[2]   Ennio Macchi and Marco Astolfi. *Organic Rankine Cycle Power Systems: Technologies and Applications*. 1st Ed. Woodhead Publishing, 2017.

[3]   Michael J. Moran, Howard N. Shapiro, Daisie D. Boettner, and Margaret B. Bailey. *Principles of Engineering Thermodynamics*. 8th Ed. Wiley, 2015.

[4]   Ding-Yu Peng and Donald B. Robinson. "A New Two-Constant Equation of State". In: *Industrial & Engineering Chemistry Fundamentals* 15 (1976), pp. 59–64.

[5]   Aspen Technology. *HYSYS 2004.2 Operations Guide*. English. Version 2004.2. AspenTech. October 2005.

[6]   Bernard Aoun. "Micro Combined Heat and Power Operating on Renewable Energy for Residential Building". PhD thesis. Ecole Nationale Supérieure des Mines de Paris, 2008.

[7]   Stefano Clemente. "Small Scale Cogeneration Systems Based on Organic Rankine Cycle Technology". PhD thesis. Università degli Studi di Trieste, 2013.

[8]   Alberto Serena. "A Multiphase Pump Experimental Analysis". PhD thesis. Norges Teknisk-Naturvitenskapelige Universitet, 2016.

[9]   Stephen R. Turns and Daniel C. Haworth. *An Introduction to Combustion: Concepts and Applications*. 4th Ed. McGraw Hill, 2021.

[10] MathWorks. *MATLAB R2020A*. https://www.mathworks.com/products/matlab.html. Version R2020A. 2020.

[11] David G. Goodwin, Raymond L. Speth, Harry K. Moffat, and Bryan W. Weber. *Cantera: An Object-oriented Software Toolkit for Chemical Kinetics, Thermodynamics, and Transport Processes*. https://www.cantera.org. Version 2.5.1. 2021.

[12] CRECK Modeling Group. *The Chemical Reaction Engineering and Chemical Kinetics Lab*. 2021. URL: http://creckmodeling.chem.polimi.it (visited on 05/30/2021).

[13] Uni Study Guides (UNSW). *Power Plant Analysis (Vapour Cycles)*. 2021. URL: http://www.unistudyguides.com/wiki/Power_Plant_Analysis_(Vapour_Cycles) (visited on 05/30/2021).

[14] Alessandro F. Castelli. "Optimization of ORCs for Low Grade Heat Recovery: Working Fluid Selection, Methodology and Applications". MA thesis. Norges Teknisk-Naturvitenskapelige Universitet, 2017.

[15] Juan Sebastian Lopez-Echeverry, Simon Reif-Acherman, and Eduard Araujo-Lopez. "Peng-Robinson equation of state: 40 years through cubics". In: *Fluid Phase Equilibria* 447 (2017), pp. 39 –71.

[16] NIST. *Reference Fluid Thermodynamic and Transport Properties Database*. `https://www.nist.gov/srd/refprop`. Version 9.1. 2013.

[17] Keith Wait, Paul M. Brown, Johannes Lux, Chris Muzny, and Eric Lemmon. *refpropm Thermophysical Properties of Pure Substances and Mixtures*. `https://trc.nist.gov/refprop/LINKING/Linking.htm`. Version 9.1. 2013.

[18] Rubin Battino, Timothy Rettich, and Toshihiro Tominaga. "The Solubility of Nitrogen and Air in Liquids". In: *Journal of Physical and Chemical Reference Data* 13 (1984), pp. 563–600.

[19] Wenjie Qi, Jingyu Ran, Ruirui Wang, Xuesen Du, Jun Shi, and Mingchu Ran. "Kinetic mechanism of effects of hydrogen addition on methane catalytic combustion over Pt(111) surface: A DFT study with cluster modeling". In: *Computational Materials Science* 111 (2016), pp. 430 –442.

[20] Gregory P. Smith, David M. Golden, Michael Frenklach, Nigel W. Moriarty, Boris Eiteneer, Mikhail Goldenberg, C. Thomas Bowman, Ronald K. Hanson, Soonho Song, Jr. William C. Gardiner, Vitali V. Lissianski, and Zhiwei Qin. *GRI-MECH 3.0*. 2020. URL: `http://combustion.berkeley.edu/gri-mech/` (visited on 12/28/2020).

[21] Eliseo Ranzi, Alessio Frassoldati, Alessandro Stagni, Matteo Pelucchi, Alberto Cuoci, and Tiziano Faravelli. "Reduced Kinetic Schemes of Complex Reaction Systems: Fossil and Biomass-Derived Transportation Fuels". In: *International Journal of Chemical Kinetics* 46.9 (2014), pp. 512–542.

[22] Eliseo Ranzi, Carlo Cavallotti, Alberto Cuoci, Alessio Frassoldati, Matteo Pelucchi, and Tiziano Faravelli. "New reaction classes in the kinetic modeling of low temperature oxidation of n-alkanes". In: *Combustion and Flame* 162.5 (2015), pp. 1679 –1691.

[23] Ghobad Bagheri, Eliseo Ranzi, Matteo Pelucchi, Alessandro Parente, Alessio Frassoldati, and Tiziano Faravelli. "Comprehensive kinetic study of combustion technologies for low environmental impact: MILD and OXY-fuel combustion of methane". In: *Combustion and Flame* 212 (2020), pp. 142 –155.

[24] Forman A. Williams. *Combustion Theory*. 2nd Ed. Addison-Wesley, 1985.

[25] Lawrence F. Shampine and Mark W. Reichelt. "The MATLAB ODE Suite". In: *SIAM Journal on Scientific Computing* 18 (1997), pp. 1 –22.

[26] David G. Goodwin, Raymond L. Speth, Harry K. Moffat, and Bryan W. Weber. *Cantera Documentation*. 2021. URL: `https://cantera.org/documentation/index.html` (visited on 05/30/2021).

[27] Warumporn Pejpichestakul, Eliseo Ranzi, Matteo Pelucchi, Alessio Frassoldati, Alberto Cuoci, Alessandro Parente, and Tiziano Faravelli. "Examination of a soot model in premixed laminar flames at fuel-rich conditions". In: *Proceedings of the Combustion Institute* 37 (2019), pp. 1013–1021.

[28] Gordon E. Andrews and Derek Bradley. "The burning velocity of methane-air mixtures". In: *Combustion and Flame* 19 (1972), pp. 275–288.

Appendix

Masteroppgåve Håkon Dalbakken, våren 2021

Tryggleik ved organiske Rankine-syklusar (ORC) med brennbare arbeidsmedium
Safety aspects of organic Rankine cycles (ORC) with combustible working fluids

Bakgrunn
Meir strev for utnytting av varme ved låg/middels temperatur til kraftproduksjon har ført til auka interesse for og bruka av organiske Rankine-syklusar. Desse syklusane brukar brennbare arbeidsmedium. For å unngå mogeleg lekkasje av luft inn i arbeidsmediet vert ofte minimums-trykket i syklusen sett litt over atmosfæretrykket. Sidan dette avgrensar den mogelege verknadsgraden til syklusen, er det interessant å undersøke dei potensielle skadane av slike lekkasjar.
Hovudproblemet kan ein sjå som tredelt: 1) Korleis ytinga til ein syklus vert påverka av luft som lek inn i arbeidsmediet. 2) Kor mykje luft som kan blandast inn i arbeidsmediet før syklusen stoggar på grunn av at eigenskapane til mediet er endra. 3) Forbrennings-eigen-skapane til luft-blanda arbeidsmedium.
Masteroppgåva er framhald av prosjektoppgåva 2020 og knytt til HighEff – Forskingssenter for miljøvennleg energi (FME) oppretta av Sintef og NTNU saman med partnarar i næringsliv, akademia og forvaltning.

 I oppgåva skal studenten
* Skaffe seg innsikt i teori og tidlegare arbeid om forbrenning, tenning og flammegrenser. Skaffe seg kunnskap om syklus-analyse og ulike, aktuelle organiske arbeidsmedium. Leite etter eventuelle tidlegare arbeid om brann/eksplosjons-fare ved luftlekkasje inn i arbeidsmedium.
* Bruke programvare, til dømes Cantera, for å rekne på laminære forblanda flammer og tenning av ulike blandingar av arbeidsmedium/luft. Kombinere dette med syklus-analyse for å kartlegge aktuelle samansetjingar og tilstandar for slike blandingar.
* Presentere arbeidet og drøfte resultata i form av ein vitskapleg rapport.

Ein framdriftsplan (planlagde aktivitetar med tidsplan) for prosjektet må leggast fram for rettleiar for kommentarar og drøfting innan 14 dagar.